

**Reviewer 1 (PGK)**

We would like to warmly thank the reviewer 1 (PGK) for this very supportive review and we are very glad that the paper was found enjoyable and attractive!...Here below is how we responded to the specific comments.

<b>Comment</b>	<b>Response</b>
P5556 line 9: somewhere here it would be useful to clarify whether this core reaches what might be considered to be the bed. I know this is tricky since the glacier-substrate interface is not clearcut in this environment, but it would be nice for the authors to be clear about whether they think there is any more “glacier” below the level reached by the drill, or if this really was the bottom.	Done. See edited manuscript
P5556 line 21-23: This sentence will confuse some readers as to whether the signature was open or closed or both at once or both but in different locations. Could be re-written for clarity.	Done. See edited manuscript
P5557 line 23: Could be re-written for clarity. Unclear whether there were 58 deep ice cores along the DEW line.	Done. See edited manuscript
P5558 line 23: Spelling of traditionally.	Replaced by practically
P5559 line 12: readers might appreciate clarification as to why the top of the basal ice is defined in these different ways by the authors and the NEEM community.	Done. See edited manuscript
P5559 line 21: events (plural)?	Done
P5570: This is one of several pages where the problem arises that there are so many abbreviation initials that readers might sometimes struggle to keep track. Here we have BIL, EPICA, EDC, PMP, CIS, NEEM, TGC... sometimes a reminder of the full label for some of those created for this paper would help the reader.	We fully agree, and this is indeed probably the page where the problem is the most obvious: <ul style="list-style-type: none"><li>- MWL has been written in full</li><li>- CIS was already defined in full in the title 422</li><li>- NEEM is the subject of the paper</li><li>- M/R is redefined now in the text</li><li>- TGC is now written in full</li><li>- BIL is written in full</li><li>- pmp has been expanded on first appearance</li></ul>
P5578 line 27-29: here, or earlier, it would be interesting to see the authors identify explicitly the exact tests that could be applied to test the different aspects of the model that they have presented.	We have now elaborated on this. See edited manuscript.

They mention some test techniques here; it would be interesting to hear exactly what the authors imagine these tests could exactly demonstrate.	
---	--

## Reviewer 2 (Simon Cook)

We thank reviewer 2 for having carefully read the manuscript and refocused our work on previous studies and classification exercises. Here below is how we responded to the specific comments.

Comment	Response
Abstract L1: I don't like this definition of basal ice. Firstly, Basal ice is not an expression – these are just 2 words in a sentence. 'Basal ice' could be an expression. Basal ice (italicized) could be and expression. Secondly, basal ice may or may not contain debris, let alone debris in layers, so the definition presented here is flawed. The inclusion of debris is not a defining characteristic of basal ice – basal ice occurs at or close to the ice-bed interface and is conditioned by processes acting at or near the glacier bed. Knight (1997) QSR gives a good definition.	We agree that the definition used is inherited from a “traditional” pragmatic view of what basal ice is. Presence of solid inclusions is indeed still the criteria used in the ice core community to decide where to change procedure for the ice sampling and sharing between teams. We also agree that we should avoid spreading confusion by multiplying definitions, and therefore extended this introductory sentence of the abstract to something very close to P. Knight's definition.
Abstract L2-3: The work undertaken in this study may represent a unique opportunity, but does the study of basal ice as a whole (in all cases, at all ice masses) represent a unique opportunity? I think you mean the former rather than the latter and should re-phrase accordingly.	We actually wanted to be more general... option 2... so text changed accordingly
Abstract L6: You've missed out the particle size work in your list of tasks.	Thanks. Text amended accordingly
Abstract L9: “were retrieved” –change to ‘was’	Done
Abstract L 10: The use of the term “specks” could be problematic. We now have a range of terms in basal ice research to define similar forms – clots, blebs, dispersed aggregates and particles, etc etc. One of the key problems in basal ice research is the proliferation of terms to define descriptively similar features or facies – see Hubbard et al. (2009) for a (relatively) recent discussion. Adding the term “specks” to an already crowded dictionary of terms could be regarded as unhelpful if you want to facilitate comparison of your work with that of others. Do you even need the term “specks”? Why not “Clear ice with particulate inclusions (CIPI – for example)? The specks and particulate	Well, again we agree with the referee that we should not multiply the proliferation of terms to describe basal ice facies. However, we really want to underline here that the amount of particulate material in each inclusion is very small, and that therefore these inclusions are also very small (needle-head like). We therefore would like to keep the “speck” terminology (which we used before e.g. in our 2015 paper), according to Myriam Webster definition “very small amount” ...To us, “specks” and “particulate inclusions” do not say the same thing...

inclusions essentially say the same thing anyway, so you are double-naming the facies.	We have added “(very small amount)” in the text to clarify
L20: The finding that CIS ice could extend the palaeoclimatic record in the ice core is a major finding, yet you don’t mention it in the conclusions!	Well, CIS has already lost a significant part of its total gas content, so what we actually meant there is that <u>part</u> of the climate signal <u>could have been</u> preserved...the text has been corrected accordingly
P5557 L6-7: Again, this definition of basal ice is flawed – see above. Basal ice is ice conditioned by processes operating at or near to the bed. This interaction with the bed is commonly manifest as inclusion of debris, sometimes in layers, but basal ice facies vary greatly in character.	Text modified accordingly
P5557, L26: Change “to access” to ‘in accessing the bedrock’	Done
P5557-8: You mention that several mechanisms for basal ice formation have been reviewed in Hubbard and Sharp (1989) and Knight (1997). However, since these papers were published, other mechanisms have been discovered to be important. For example, glaciohydraulic supercooling (Alley et al., 1998; Lawson et al., 1998 – in J Glac; Cook et al., 2006 – in Progress in Physical Geography) and porewater freeze-on beneath ice streams (Christoffersen and Tulaczyk, 2003 and Christoffersen et al., 2006 – J. Geophys. Res.). It might be appropriate, therefore, to cite the most up-to-date review of basal ice by Hubbard et al (2009) at this point.	We fully agree that this referencing was too narrow! Thank you very much and apologies for that. The reference list has now been expanded.
P5558, L13. Change “were” to ‘was’	Done
P5558, L17. Change “referred” to ‘referred to	Done
P5558, L19. Change “timer” to ‘time’	Done
P5558, L23. Spelling of ‘traditionally’	Done
P5558, L24. I appreciate that the Tison et al. (2015) has set a precedent here in terms of the definition of basal ice, but I maintain that this definition is flawed. Basal ice does not always contain debris or any significant amount of debris.	One of the main constrain here is that the sampling protocole of the NEEM ice core, not knowing “a priori” the upper boundary of the basal ice layer as defined previously, needed some visual criteria to adapt the sampling scheme. We have replaced “traditionally” by “practically” and now stated that constrain in the text.
P5559, L29: change “event” to ‘events’	Done
P5560, L8. Spelling of ‘Vienna’	Done
P5560, L9. Spelling of ‘series’	Done
P5560, L11. Spelling of ‘ensure’	Done
P5561, L11. Here and throughout. Whether or not you take my advice about the naming of	We have chosen the second option, since we are not always convinced of the

<p>your ice facies (specks), it would be useful to either harmonise your classification with that of Hubbard et al (2009), or to provide in the text a statement about which of the ice types outlined in Hubbard et al.'s scheme your facies are equivalent to. You do this for DRL ice, but not for the other facies.</p>	<p>"easiness of use" of the classification in Hubbard et al; (2009). The latter indeed combines layer thickness, particle density, particle distribution infos in each basal ice cryofacies, which we believe still do not cover adequately all possible facies. Scales are really a hard part too. We have however carefully given what we thought would be a good equivalent of our ice types in the Hubbard et al. 2009 classification in the description of section 3.1.</p>
P5562, L12: add 'particles' after "debris".	Done
P5562, L14: change "evidences" to 'evidence'	Done
P5566 L10-11: For your information, Cook et al (2010) in Boreas used freezing slopes of both cold and open systems to define an envelope of all possible isotope compositions involved in basal ice formation – might be a useful reference to cite here given that you have used a similar approach.	Thank you. We must admit we have missed that one. It is now included. We guess this is in fact Cook et al., 2009 in Boreas?
This would also apply for P5567 L9-10.	See above
P5566 L17: change "biases" to 'bias'	Done
P5567 L15: change "exercice" to 'exercise'	Done
P5568 L17: change "combination" to 'combinations'	Done
P5569 L15: spelling of 'developed'.	Done
P5570 L18-20: I couldn't make sense of this sentence	We have rephrased that sentence
P5571 L10-14: I couldn't make sense of this sentence.	We have rephrased that sentence
P5573 L24: For your information, Waller et al. 2000 Quat Sci Rev and Cook et al. (2011) J. Glac, both discuss the potentially important, yet probably under-estimated, role of tectonic mixing in the generation and metamorphism of basal ice.	We have added these two references too. Thank you so much.
P5574 L4: spelling of 'literature'	Done...actually p.5575 (?)
P5574 L24: change 'moraine' to 'till'	Done
P5578 L15: change "litterature" to 'literature'	Done
Fig 1 caption: I suggest rewording this – "three contrasting visual ice types" doesn't really mean anything. I think you mean 'three visually contrasting ice types'.	Done
Fig 3 caption. Change 'cumulated' to 'cumulative'. What is "volume density"? I'm sure this is something that the granulometer generates, but it seems an odd term.	It is a volume % of a given fraction taking density (the ratio of volumic mass of the particle to the volumic mass of the liquid, taking into account the nature and physical properties of the liquid) into account; the caption has been amended.

Fig 5. I appreciate the desire to present all information together in this diagram for direct comparison, but there are so many datapoints and lines that some information is obscured. Is it worth considering presenting multiple graphs? Perhaps with a combined graph too as you already have? Or even a “final” graph that just shows the lines of best fit after presenting individual graphs for each dataset.

We agree with the referee. We have produced a new “3 pannels” figure for clarity.

**Small corrections from authors for clarity**, are highlighted in grey

# A comprehensive interpretation of the NEEM basal ice build-up using a multi parametric approach.

T.Goossens<sup>1</sup>, C. J. Sapart<sup>1,2</sup>, D. Dahl-Jensen<sup>3</sup>, T. Popp<sup>3</sup>, S. El Amri<sup>1</sup> and J.L. Tison<sup>1</sup>.

[1] {Laboratoire de Glaciologie, Université Libre de Bruxelles, 1050 Brussels, Belgium}

[2] {Institute for Marine and Atmospheric Research Utrecht, Utrecht University, 3584CC Utrecht, The Netherlands}

[3] {Centre for Ice and Climate, Niels Bohr Institute, University of Copenhagen, 2100 Copenhagen, Denmark}

Correspondence to: T. Goossens ([tgoossen@ulb.ac.be](mailto:tgoossen@ulb.ac.be))

## Abstract

*Basal Ice* is a common expression to describe bottom ice layers of glaciers, ice caps and ice sheets in which the ice is primarily conditioned by processes operating at the bed. It is chemically and/or physically distinct from the ice above, and can be characterized by a component of basally derived sediments. The study of basal ice properties provides a rare opportunity to improve our understanding of subglacial environments and processes and to refine ice sheet behaviour modelling. Here, we present and discuss the results of water stable isotopes ( $\delta^{18}\text{O}$  and  $\delta\text{D}$ ), ice fabrics, debris weight/size distribution and gas content of the basal part of the NEEM (North Greenland Eemian Ice Drilling Project) ice core. Below a depth of 2533.85 m, almost 10 m of basal debris-rich material were retrieved from the borehole and regular occurrence of frozen sediments with only interstitial ice lenses in the bottom 5 meters, suggest that the ice-bedrock interface was reached. The sequence is composed of an alternation of three visually contrasting types of ice: clear ice with specks (very small amounts) of particulate inclusions, stratified debris-rich layers, and ice containing dispersed debris. The use of water stable isotope signatures ( $\delta^{18}\text{O}$  and  $\delta\text{D}$ ) together with other parameters, allows to discriminate between the different types of ice and to unravel the processes involved in their formation and transformation. The basal debris-rich material presents  $\delta^{18}\text{O}$  values [-39.9 ‰; -34.4 ‰] within the range of the above last 300 m of unaltered meteoric ice [-44.9 ‰; -30.6 ‰] spanning a glacial-interglacial range of values. This rules out the hypothesis of a basal ice layer originating from pre-ice sheet ice overridden by the growing ice sheet (as previously suggested e.g. in the case of the GRIP ice core), since the latter would result in an heavier isotopic signature for ice formed at a much lower altitude. We show that clear basal ice with specks corresponds to altered meteoric glacial ice where some of the climatic signal could have been preserved. On the other hand, the stratified debris-rich layers and the ice containing dispersed debris layers respectively express an "open" or "closed" system melting/refreezing signature, somewhat blurred by mixing processes in the upper part of the sequence. Climatic reconstruction is therefore prohibited from these ice types. We propose a first interpretative framework for the build-up of the NEEM basal ice sequence, based on the origin of the various ice types.

## 1 Introduction

The dynamics of ice sheets and their climatic feedback and future contribution to sea level rise still remains highly uncertain (Church et al., 2013). Establishing more accurate and constrained models of ice sheet behavior has therefore become an important scientific challenge.

45 The Basal Ice Layer (BIL) of an ice-sheet, is primarily conditioned by processes operating at  
46 the bed and often contains debris-laden ice close to the ice-bedrock interface (Souchez et al.,  
47 1978). It is, according to the following description (Knight, 1997): “a rheological control on ice  
48 sheet dynamics; an indicator of subglacial conditions and processes; a limit to the downward  
49 extension of climate record from deep ice core(s)”. Because its physical and chemical  
50 characteristics are representative of the different processes leading to its formation, a multi-  
51 parametric study of the BIL offers the opportunity to infer the former thermal, rheological and  
52 environmental conditions prevailing during its formation and reveal the processes acting at  
53 the ice-bedrock interface (Hubbard and Sharp, 1995; Alley et al., 1998; Lawson et al., 1998;  
54 Christoffersen and Tulaczyk, 2003; Christoffersen, 2006; Cook et al., 2007; Hubbard et al.,  
55 2009). These inferences allow establishing better constrained initial and boundary conditions  
56 required for ice sheet modelling and bound the validity of paleoclimatic data interpretation.

57 Understanding basal ice processes is therefore an important challenge to face for those who  
58 are looking at ice older than a million years in Antarctica or trying to decipher the details of  
59 rapid climate changes in more recent times in Greenland (Fischer et al., 2013).

60 To date, only a few deep ice core projects have been conducted on the Greenland main ice  
61 divide (Dye3 - ice core locations elected at one of the 58 US radar stations of the Distant Early  
62 Warning (DEW) Line, GISP2 - Greenland Ice Sheet Project, GRIP - Greenland Ice Core Project,  
63 NGRIP - NorthGRIP) and most recently NEEM (North Greenland Eemian Ice Drilling Project).  
64 Due to difficulties in accessing the bedrock, the various processes involved in the formation of  
65 a BIL and their possible interactions are still not well understood. Previous studies  
66 summarized in two review papers (Hubbard and Sharp, 1989; Knight, 1997) have however  
67 identified a certain number of mechanisms leading to a physically distinguishable BIL.

68 Basal temperature below the pressure melting point (pmp) allows the formation and  
69 preservation of a basal ice sequence as recovered for example from the Byrd (Antarctica) and  
70 GRIP and GISP2 ice core (Gow and Meese, 1996). In other areas where the pmp is reached,  
71 paleoclimatic information could be partially melted away and lost e.g. at NGRIP (Andersen et  
72 al., 2004). In any case, interactions between moving ice and the irregular bedrock can result in  
73 flow disturbances, partial alteration of the ice properties and a loss of climate and  
74 environmental signal much higher into the ice column and well above the BIL (e.g. Landais et  
75 al., 2012; Tison et al., 2015)

76 The international NEEM project aimed to recover a complete and unaltered sequence of  
77 Eemian ice and it succeeded to reach close to the bedrock in 2011 at a depth of 2537.98 m.  
78 About 4 m of debris-rich ice was retrieved at that time (Dahl-Jensen et al., 2013). During the  
79 2011 and 2012 field seasons, a narrower borehole was drilled further through about 6 m of  
80 frozen sediment layers alternating with sparser clear ice segments containing dispersed  
81 debris. This is the second time that a complete sequence from non-altered ice originating from  
82 a firnification process (referred to here as meteoric ice - MI) to frozen sediments has been  
83 retrieved from a borehole in Central Greenland (first time being the GISP2 ice core – Gow and  
84 Meese, 1996).

85 In this paper, we use a high-resolution multiparametric approach (stable isotopes, ice fabrics,  
86 debris content and total gas content) to achieve a comprehensive interpretation of the NEEM  
87 basal ice build-up. We follow here the terminology proposed by Tison et al. (2015), in which  
88 “basal ice” practically refers to the part of the ice core showing visible solid inclusions. This is  
89 also because the sampling protocole for the NEEM ice core needed some visual criteria to  
90 adapt the sampling scheme. In this study the presence of millimetric solid inclusions in the  
91 BIL is shown to be an indicator of a transformation process resulting from interaction with  
92 the bedrock, but does not necessary mean that these inclusions originated from the ice

93 bedrock interface. The term “deep ice” is used to name the ice sequence just above, that is  
94 potentially altered by the vicinity of the bedrock, but does not show any visible inclusions.

## 95 **2 Material and methods**

### 96 **2.1 Drilling**

97 The NEEM core (77.45° N, 51.06° W) was drilled between 2008 and 2012 field seasons using  
98 the Hans-Tausen (HT) drill (9.8 mm inner diameter) (Johnsen et al., 2007) from the surface to  
99 the depth of 2537.99 m. Because of the increasing occurrence of solid particles with depth, a  
100 narrower dedicated “Rock Drill” (RD) (2.5 inner diameter) was used below this depth and the  
101 final depth of 2543.84 m was reached. For transport and storage purposes the core was cut  
102 into 55 cm sub-units called “bags”.

### 103 **2.2 Sampling and analytical methods**

104 The basal ice layer, as defined in the introduction, starts effectively at bag 4595,  
105 corresponding to a depth of 2527.25 m. However, because visible solid inclusions were only  
106 described in the field starting at 2533.85 m depth, for logistic reasons, the NEEM community  
107 has only adopted the dedicated basal sampling procedure (defining the dimensions of samples  
108 attributed to each measurement) from that depth (bag 4608) onwards, the segment which is  
109 the focus of the present study. Samples were cut using a Well 6234 diamond wire saw (Tison,  
110 1994). Due to its smaller diameter (2.5 cm) the basal cutting scheme was not applied to the  
111 RD core for which a smaller number of parameters are possibly extractable.

112 The total gas content (TGC) was measured using a Toepler pump and the melting/refreezing  
113 (M/R) extraction technique (Martinerie et al., 1994; Raynaud et al., 1983). The existence of  
114 numerous debris layers is a potential indicator of the occurrence of melting/refreezing (M/R)  
115 events (Hubbard and Sharp, 1989; Knight, 1997) that leads to a drastic depletion of the gas  
116 content. In order to insure detectable measurements, samples of 5 cm vertical resolution were  
117 measured by groups of 3 or 4. Data are expressed in milliliters of gas per kilogram of ice ( $\text{ml}_{\text{gas}}$   
118  $\text{kg}_{\text{ice}}^{-1}$ ) and the precision is estimated at  $\pm 5\%$ .

119 Melted residues from TGC samples were filtered on 0.20  $\mu\text{m}$  Millipore® filters. Collected dry  
120 residues were weighed and their content expressed as weight percentage of the ice plus  
121 debris weight. Note that the sampling resolution of debris content is therefore inherited from  
122 the TGC samples grouping.

123 Ice water isotopes were measured at the Niels Bohr Institute – Center for Ice and Climate,  
124 Copenhagen – using a Picarro 2120 Cavity Ring-Down Spectroscopy Analyser equipped with a  
125 high throughput evaporator. Data are expressed as permil (‰) difference relative to Vienna  
126 Standard Mean Ocean Water (VSMOW) and the accuracy is 0.01 ‰ for both  $\delta\text{D}$  and  $\delta^{18}\text{O}$ . The  
127 initial vertical resolution was 5 cm for the first series of samples corresponding to the ice  
128 drilled during the 2010 field season (2533.85 – 2537.30 m depth). To ensure a better  
129 detection of potential small-scale M/R events, the samples covering the 2011 and 2012 field  
130 season (below 2537.30 m) were later analysed at 2 cm vertical resolution.

131 In order to cope with the presence of debris, vertical 400 microns thin sections were prepared  
132 (resolution 5 cm) using a Well 6234 diamond wire saw (Tison, 1994) instead of the standard  
133 microtome procedure initially described in Langway (1958). C-axis orientations were  
134 obtained using a G50 Fabric Analyser (Wilson et al., 2003). The analyser generates a file  
135 containing lines of raw orientation information with quality factors at the pixel scale (1 pixel =  
136 43  $\mu\text{m}$ ). This raw dataset was post-processed using algorithms from the MTEX (Bachmann et  
137 al., 2010) and FAME (Paternell et al., 2014) MATLAB® toolboxes in order to filter the poor



138 quality pixels (threshold: quality parameter lower than 70 %) and produce stereographic pole  
139 plots in the vertical plane. The size of the crystals is revealed by pictures of cross-polarized  
140 thin-sections generated by the fabric analyser.

141 Granulometry of the incorporated debris was measured on discrete selected samples using a  
142 Malvern Mastersizer 3000® laser granulometer.

### 143 3 Results

#### 144 3.1 Ice types and debris content

145 Figure 1 displays representative samples of our classification based on the raw visual  
146 appearance of the ice types encountered in the NEEM basal ice sequence.

147 As described in sect. 2, a specific cutting procedure has been adopted from the first core  
148 encountered showing conspicuous layers of highly concentrated debris (top at 2533.850 m),  
149 following a “practical” definition of the basal ice layer. However, it was discovered “a  
150 posteriori” that the first visible solid inclusions occur further up in the core at a depth of  
151 2527.250 m. These start as scarce (a few per 55 cm “bag” core) submillimetric pinhead like  
152 inclusions, with their size and densities slowly increasing downwards. We will refer to this ice  
153 type illustrated in Fig. 1a, as “Clear Ice with Specks” CIS (white symbols in Fig. 2a). It would  
154 correspond to the lower end (in terms of debris concentration) of the *banded dispersed*  
155 cryofacies of Hubbard et al. (2009).

156 From 2533.85 m to 2536.60 m (Fig. 2a), the BIL is dominated by this ice type showing  
157 increasingly large amount of very small dark solid inclusions. The diameters of these specks  
158 range between less than one millimeter in the top and up to 3 mm downcore. Figure 3 shows  
159 the volume density (in %) and cumulated volume density (in %) for the range of size from  
160 clays to gravel for a set of representative samples from the NEEM BIL. CIS (Fig. 3a) mainly  
161 consists of silts (local maximum at 40  $\mu$ m) and small sands (local maximum at 150  $\mu$ m),  
162 which suggests that most of the specks actually consist of aggregates of individual particles.

163 Embedded in this CIS, segments of ice containing individual high concentration debris layers  
164 (second ice type, Fig. 1b, black symbols in Fig. 2a, ranging from 2 to 5 mm in thickness) were  
165 observed at depths from 2534.50 m to 2534.60 m and from 2534.85 m to 2534.87 m. In these  
166 high concentration debris-rich layers (DRL), debris size ranges from clay to coarse sand and  
167 fine gravels (Fig. 3b) and the debris weight content reaches 0.4 % (at 20 cm depth resolution -  
168 Fig. 2b).

169 A similar sequence, but with much larger DRL segments (from 1 to 12 cm in thickness) is  
170 observed between 2536.60 m and 2538.15 m (Fig. 1b, Fig. 2a). In some of these layers, the  
171 debris weight content peaks at 23 % (Fig. 2b) (at 15 cm depth resolution) and the debris size  
172 distribution resembles the one in the DRL above, with large proportion of fine sands (Fig. 3c).  
173 In one of these layers at 2536.65 m depth, a large granite pebble of 5 cm of diameter is  
174 protruding from the side of the core. A careful examination of these DRL segments (e.g. Fig.  
175 1b) shows that they generally consist of an alternation of thinner individual debris layers with  
176 clear ice laminae. This is typical of what has been referred to as the *laminated cryofacies* in  
177 (Hubbard et al., 2009) classification of basal ice types.

178 At 2537.30 m depth, a new ice type can be observed (Fig. 1c and grey symbols in Fig. 2a) that  
179 consists of clear ice containing dispersed debris (IDD) at such low concentration (typically 0.5  
180 to a few % in weight) that the ice still remains transparent. Individual debris particles are  
181 roughly aligned in laminated bands that occasionally cross-cut at low angles suggesting a  
182 folding structure (Fig. 1c). This ice type could also be classified as a *banded dispersed*  
183 cryofacies with a higher debris content than the CIS described above.

184 Along the same lines the DRL segments show **evidence** of tilting with regard to the core axis  
185 (the "vertical" ) and that the dip goes in opposite directions depending on the section  
186 considered in the BIL (Fig. 4, left vertical strip showing core in transmitted light). This  
187 observation is valid since the azimuth of the core remains coherent throughout the BIL.

188 Down to the depth of 2541.80 m, clear ice layers containing variable amount of dispersed  
189 debris alternate with more frequent layers of ice presenting high concentration debris layers  
190 (Fig. 2a). Below that depth the core mainly consists of an alternation of unsorted frozen  
191 sediments layers, **the solid cryofacies in Hubbard et al. (2009)**, and ice layers with dispersed  
192 debris (also referred to as IDD). In this section, the debris size range is similar to the DRL  
193 above with further increase of the small sand proportion (Fig. 3d). Pebbles of cm-size are  
194 regularly found in this lower part of the basal ice sequence. An irregular increasing downward  
195 trend in debris content (Fig. 2b) and debris size (Fig. 3) is observed along the NEEM basal ice  
196 core.

### 197 **3.2 Gas content**

198 The TGC versus depth profile of the NEEM BIL shows a generally increasing trend from the  
199 top to the bottom of the sequence (Fig. 2c). The lowest value ( $0.30 \text{ ml}_{\text{gas}} \text{ kg}_{\text{ice}}^{-1}$ ) is observed in  
200 the upper part of the core where the TGC is quite constant around  $1 \text{ ml}_{\text{gas}} \text{ kg}_{\text{ice}}^{-1}$  (from 2533.85  
201 m to 2536.60 m).

202 At intermediate depths (2536.60 m – 2539.19 m), the TGC is more variable with slightly  
203 higher values fluctuating around  $4 \text{ ml}_{\text{gas}} \text{ kg}_{\text{ice}}^{-1}$ . The lowest part of the core is characterized by  
204 TGC up to 5 times higher than measured in the upper layers and reaches a maximum observed  
205 value of  $56.17 \text{ ml}_{\text{gas}} \text{ kg}_{\text{ice}}^{-1}$  at 2539.25 m of depth.

206 Close to the bottom, the TGC is similar to the one at intermediate depth. The deepest sample  
207 (2543.25 m) reaches a second maximum of  $33.25 \text{ ml}_{\text{gas}} \text{ kg}_{\text{ice}}^{-1}$ .

208 The mean TGC value of the entire NEEM BIL ( $6.19 \text{ ml}_{\text{gas}} \text{ kg}_{\text{ice}}^{-1}$ ) is very low compared to the  
209 typical dry-firn derived meteoric ice (MI) value of about  $90 \text{ ml}_{\text{gas}} \text{ kg}_{\text{ice}}^{-1}$  (Martinerie et al., 1994;  
210 Raynaud et al., 1983).

### 211 **3.3 Stable isotope composition**

212 The depth profiles of the ice-water isotopes of the NEEM basal ice core are shown in Fig. 2d  
213 with  $\delta\text{D}$  and  $\delta^{18}\text{O}$  expressed in permil (‰) versus the Vienna Standard Mean Ocean Water (V-  
214 SMOW). The various symbols in Fig. 2d refer to the different visual ice types identified above  
215 with CIS as white circles, DRL as black triangles and IDD as grey squares.

216 With a mean value of  $-38.4 \text{ ‰}$ , the  $\delta^{18}\text{O}$  profile displays a non-linear downward trend towards  
217 an isotopic enrichment in heavy isotopes (i.e. increasing  $\delta$ -values).

218 Along the first 2.8 m of the core where 5 cm resolution measurements were performed,  $\delta^{18}\text{O}$   
219 values slightly fluctuate around  $-39.0 \text{ ‰}$  with two layers enriched by about  $1 \text{ ‰}$  in heavy  
220 isotopes at 2534.60 m and 2535.65 m depth.

221 From 2536.60 m to 2537.15 m, the ice shows a progressive depletion in heavy isotopes and  
222 reaches the lowest value measured in  $\delta^{18}\text{O}$  ( $-39.9 \text{ ‰}$ ) at 2537.15 m of depth.

223 Between 2537.15 m and 2537.90 m, the  $\delta^{18}\text{O}$  profile is nearly constant and its values are again  
224 clustered around  $-39.0 \text{ ‰}$ .

225 From 2537.90 m depth to 2539.31 m, the  $\delta^{18}\text{O}$  profile shows a positive trend towards isotopic  
226 enrichment and larger amplitude variations with a difference of about 3.5 ‰ between the  
227 lowest value (-39.9 ‰) and the locally most enriched layer (-35.5 ‰), respectively at  
228 2537.17 m depth and 2538.14 m depth.

229 Finally, the deepest samples (below 2543.15 m) are characterized by the highest  $\delta^{18}\text{O}$  values  
230 recorded in the NEEM BIL with a maximum of -34.4 ‰. These remain well in the range of  
231  $\delta^{18}\text{O}$  values observed in the ice above the BIL (last 300 m depth interval above the BIL, Fig. 5,  
232 dark crosses).

233 The  $\delta\text{D}$  profile follows the same pattern as the  $\delta^{18}\text{O}$  with a mean value of -301 ‰ and it  
234 ranges from -311 ‰ (at 2536.85 m depth) to -275 ‰ (at 2543.15 m depth).

### 235 **3.4 Ice textures and Fabrics**

236 Textures and fabrics have only been investigated on the basal ice sequence drilled during the  
237 2010 field season, which represents 3.45 m of material represented by the green line on the  
238 right of Fig. 2a. A detailed view of this sequence is presented in Fig. 4.

239 Large interlocking crystals (up to 15 cm equivalent diameter) are representative of clear ice  
240 layers while small crystals (less than 1 cm equivalent diameter) are always found in the  
241 debris layers.

242 As shown by the c-axis pole diagrams (summarized in the last column of Fig. 4,) the two types  
243 of ice crystals show strikingly different fabrics. Large crystals are organised in such a way that  
244 their fabric shows a small girdle roughly centered around the core axis, while small crystals  
245 plot as a single maximum along the same direction. Surprisingly, a third type of generally  
246 small crystals, frequently occurs along the sides of the ice core (e.g. see thin section at a depth  
247 of 2536.40 m in Fig. 4). The fabric of these border crystals partly mimics the pattern of the  
248 populations of small and large crystals, but also add randomness to the distribution. Note that  
249 these border crystals are part of the ice core and do not represent the expression of “water-  
250 welding” during the thin sectioning procedure.

251

## 252 **4 Discussion**

253 During ice formation the basal sequence has lost an important part of its gas content and  
254 contains numerous debris layers. This study is based on a co-isotopic approach in order to  
255 test if processes involving melting/refreezing (M/R) events, able to reject gases and  
256 incorporate the coarser particles in the observed debris range, could be responsible for the  
257 build-up of the sequence or at least parts of it.

### 258 **4.1 A $\delta^{18}\text{O}_{\text{ice}} - \delta\text{D}_{\text{ice}}$ approach to detect melting/refreezing processes**

259 Figure 5 shows the  $\delta^{18}\text{O}_{\text{ice}} - \delta\text{D}_{\text{ice}}$  relationship for the various ice types described in sect. 3.1,  
260 and compares it to the co-isotopic signature of the 567 samples of meteoric ice (MI) from the  
261 300 meters above (dark crosses). Samples of MI are aligned on a slope of 8.02 which is typical  
262 of the global Meteoric Water Line (MWL) (Craig, 1961).

#### 263 **4.1.1 The “freezing slope” concept and caveats**

264 On a co-isotopic diagram, a M/R process can be detected by a slope of the  $\delta^{18}\text{O}_{\text{ice}} - \delta\text{D}_{\text{ice}}$   
265 relationship for a group of samples significantly lower than 8, in accordance with what is  
266 usually referred to as a “freezing slope”. A freezing slope is the result of a fractionation effect

267 between light and heavy isotopes in the course of freezing. Jouzel and Souchez (1982) have  
 268 theoretically computed the value of the freezing slope in the case of a closed system reservoir  
 269 ( $S_{CS}$ ) and successfully validated it on an experimental setup (Souchez and Jouzel, 1984). It is  
 270 expressed as:

$$271 \quad S_{CS} = \frac{(\alpha-1) (1000+\delta D_{res})}{(\beta-1) (1000+\delta^{18}O_{res})} \quad (1)$$

272 where  $\alpha$  (=1.0212) and  $\beta$  (=1.00291) are the equilibrium fractionation coefficients between  
 273 water and ice for D/H and  $^{18}O/^{16}O$  respectively (Lehmann and Siegenthaler, 1991) and  $\delta^{18}O_{res}$   
 274 and  $\delta D_{res}$  are the initial isotopic composition of the reservoir before freezing. In the basal part  
 275 of an ice sheet, the meltwater supplying a freezing reservoir most presumably originates from  
 276 the meteoric ice above. As no isotopic fractionation occurs during melting (Friedman et al.,  
 277 1964; Souchez and Lorrain, 1991),  $\delta^{18}O_{res}$  and  $\delta D_{res}$  are located on the MWL, i.e. at the  
 278 intersection with the best fit line across the samples resulting from the freezing process.

279 Several studies have used this concept of the “freezing slope” to track M/R processes in basal  
 280 ice sequences of ice sheets (Knight, 1989; Hubbard and Sharp, 1993, 1995; Iverson and  
 281 Souchez, 1996; Souchez et al., 1988, 1994, 1998; Cook et al., 2009; Larson et al., 2010) by  
 282 comparing the  $\delta^{18}O_{ice}-\delta D_{ice}$  regression line of their set of samples to the modelled freezing line,  
 283 using closed system eq. (1) with the initial values for the freezing meltwater provided by the  
 284 intersection of the  $\delta^{18}O_{ice}-\delta D_{ice}$  regression line through the samples with the MWL. These  
 285 attempts were only partly successful due to various potential sources of bias summarized  
 286 below and in Fig. 6:

287 a. The vertical sampling resolution may affect the detection of a M/R signature. To pinpoint  
 288 any isotopic fractionation in a sample, its vertical size must be smaller than the one of the  
 289 refreezing process (Souchez et al., 1988). If a single sample covers the full set of refreezing  
 290 increments, its measured  $\delta$ -value corresponds to the average  $\delta$ -value of all the increments  
 291 together. Because this average is equal to the meteoric  $\delta$ -value of the initial reservoir  
 292 admitted to freeze ( $\delta^{18}O_{res}$  and  $\delta D_{res}$ ), no isotopic fractionation is detected (Fig. 6, case a).

293 b. Equation (1) is only valid for “closed system” freezing. In nature, it is possible that the  
 294 system is “open” both in terms of refrozen ice/meltwater ratio and in terms of the water  
 295 isotopic signature. This more complex case has been discussed (Souchez and De Groot, 1985;  
 296 Souchez, 1984) and provides the following expression for the “open system” freezing slope  $S_{OS}$   
 297 (Fig. 6, case b):

$$298 \quad S_{OS} = \frac{\alpha(\alpha-1) (1000+\delta D_{res}) - \frac{A}{F} (\delta D_{inp} - \delta D_{res})}{\beta(\beta-1) (1000+\delta^{18}O_{res}) - \frac{A}{F} (\delta^{18}O_{inp} - \delta^{18}O_{res})} \quad (2)$$

299 where  $\delta^{18}O_{res}$  and  $\delta D_{res}$  are the isotopic composition of the water reservoir before freezing and  
 300  $\delta^{18}O_{inp}$  and  $\delta D_{inp}$  are the isotopic composition (considered constant) of the input water joining  
 301 the reservoir in the course of freezing. A and F are respectively the constant input and  
 302 freezing rate. While the closed system approach provides a single theoretical freezing slope,  
 303 the open system model usually provides a set of multiple possible freezing slopes, the range of  
 304 which is constrained by generally unknown values of  $\delta_{inp}$  and A/F. Given the numerous  
 305 possible freezing slopes it provides, the open system approach increases the probability of  
 306 finding a fit that describes sufficiently the observations, making it a less parsimonious model.  
 307 The sensitivity of the basal ice isotopic signature to the range of isotopic values of the input  
 308 water and to the “degree of closure” of the system (ratio A/F) has been discussed in previous  
 309 modelling exercises (Hubbard and Sharp, 1995; Cook et al., 2009). The authors concluded

310 that a freezing slope might not be displayed, and suggested that only a range of plausible  
311 values for the input waters can be deduced from the observed isotopic signature of the ice.

312 c. If the vertical sampling resolution is too coarse, it could also possibly lead to measurements  
313 that mix both M/R and meteoric signals. In such situations, samples might be located on  
314 intermediate positions between the MWL and the freezing line, their precise coordinates  
315 depending on both the proportion and values of each of the co-isotopic signals they combine.  
316 Such a process has a higher probability to result in a more scattered distribution between  
317 theoretical freezing slopes and the MWL (Fig. 6, case c). A similar case could be drawn for a  
318 mixing process with a “closed system” freezing slope.

#### 319 4.1.2 Tracking M/R in the NEEM basal ice

320 In the following sections, we will use analyses of covariance techniques (ANCOVA), to track  
321 M/R processes in our various ice types from the NEEM basal ice. The rationale is as follows:  
322 For each group of observations, a regression line is calculated with slope  $S_{obs}$  (Table 1a). At  
323 first,  $S_{obs}$  is compared to the slope of the MWL ( $S_{MWL}$ ). The M/R origin hypothesis is refuted if  
324 both slopes are not significantly different (P-value > 0.01). However if  $S_{obs}$  is significantly  
325 lower than  $S_{MWL}$  (P-value  $\leq$  0.01), the considered group of samples could presumably originate  
326 from a M/R process. This assumption is further tested by comparing  $S_{obs}$  with the expected  
327 closed system slope ( $S_{CS}$ ) computed from eq. (1) with the intersection between the observed  
328 regression line and the MWL being the initial water  $\delta$ -values for the freezing process (Table  
329 1b). The closed system M/R origin hypothesis is accepted for that group of samples if the two  
330 slopes are not statistically different. If  $S_{obs}$  is both statistically different from  $S_{MWL}$  and  $S_{CS}$  or if  
331 no significant regression line can be drawn for that specific group, then alternatives b) and c)  
332 in sect. 4.1.1 and figure 6 have to be considered.

333 Table 1 summarizes the observed regression lines for each group of basal ice samples defined  
334 in sect.3 (and a few other combinations, see below - Table 1a) and the theoretical closed  
335 system freezing lines calculated for the various groups (Table 1b). These data are used in the  
336 following section to discuss the origin for the various groups, in conjunction with the other  
337 available ice properties.

### 338 4.2 Origin of the ice types

#### 339 4.2.1 Whole basal ice sequence

340 Since the whole basal ice sequence displays a stacking of clear ice and debris bands, one could  
341 assume that the whole sequence might have resulted from a large scale M/R process such as a  
342 “bulk freezing-on” mechanism (e.g. at transitions from warm to cold bed conditions under the  
343 ice sheet) (Weertman, 1961). The corresponding  $\delta^{18}O_{ice} - \delta D_{ice}$  slope for the whole set of basal  
344 ice samples ( $S_{obs-BIwhole} = 6.48$ , Table 1a) is significantly lower (P-value = 0) than that of the  
345 Meteoric Water Line ( $S_{MWL} = S_{MI300} = 8.02$ ), excluding a meteoric origin for the whole  
346 sequence. A closed-system M/R origin hypothesis is highly unlikely because  $S_{obs-BIwhole}$  is  
347 significantly higher (P-value = 0.001) than the slope computed from the intersection between  
348  $S_{obs-BIwhole}$  and the MWL, referred as  $S_{BIwhole \cap MI300}$  (= 5.20, Table 1b). This and the contrasted  
349 properties (Fig. 1 to 4) within the sequence suggest that it should indeed not be considered as  
350 a single refrozen entity, but rather interpreted as a composite signal.

#### 351 4.2.2 Clear Ice with Specks (CIS)

352 The slope of the  $\delta^{18}O_{ice} - \delta D_{ice}$  regression line for the CIS samples ( $S_{obs-CIS} = 7.93$ , Fig. 5a and  
353 Table 1a) is not significantly lower (P-value = 1) than the slope of the Meteoric Water Line

354 ( $S_{MI300} = 8.02$ ). This similarity suggests that M/R events at a scale larger than the resolution of  
355 the samples (5 cm) did not occur for this ice type. This is further confirmed by  $S_{obs-CIS}$  being  
356 significantly too high (P-value = 0) compared to the expected  $S_{CS-CIS}$  (3.85) that would have  
357 been developed from melted meteoric ice (MI) with  $\delta$ -values (-64.4 ‰; -506 ‰) at the  
358 intersection with the CIS regression line (totally unrealistic value lying well out of the range of  
359 the whole NEEM core - Fig. 5a).

360 The rejection of the Melting/Refreezing (M/R) hypothesis for the CIS samples is coherent with  
361 their textural signature. As shown in Fig. 4, the large crystals of the clear ice samples with  
362 specks show a typical small girdle around the core axis. This is similar to the recrystallization  
363 fabric described higher up in the core in the Eemian “warm” ice (Montagnat et al., 2014). This  
364 “inherited” strain history is not compatible with melting-refreezing processes that would have  
365 reset the signature to smaller grains oriented according to the simple shear stress regime  
366 dominating in the deepest layers of the ice sheet (Cuffey and Paterson, 2010; Hooke and  
367 Hudleston, 1980).

368 Despite the fact that the isotopic and textural signature of the CIS samples are in accordance  
369 with a meteoric ice origin, they show a very low Total Gas Content (TGC mean value = 1.46  
370  $ml_{gas} kg_{ice}^{-1}$ , ranging from 0.30 to 5.42  $ml_{gas} kg_{ice}^{-1}$ , Fig. 2c) as compared to typical ice sheet  
371 meteoric ice values (ca. 90  $ml_{gas} kg_{ice}^{-1}$ ). This points to mechanical “reworking” close to the ice-  
372 bedrock interface. As discussed for the Basal Ice Layer of EPICA Dome C (EDC) (Tison et al.,  
373 2015), an intense migration recrystallization process in ice close to the pmp results in  
374 drastically increased crystal sizes and expulsion of gases and impurities out of the crystal  
375 lattice into the intergranular liquid network. As impurities get concentrated within the  
376 premelt layer, they are shown to form precipitated aggregates leading to an ice type very  
377 similar to our CIS. A major difference, is that, in the EDC basal ice, typical meteoric TGC are  
378 preserved. Note that the EDC ice core was terminated at least a few tens of meters above the  
379 ice-bedrock interface. It is therefore possible that, at NEEM, the CIS has travelled close enough  
380 to the ice-bedrock interface for its TGC to be partially expelled out of the crystal lattice and  
381 drained with the intercrystalline interstitial water (premelt) towards the bedrock. This  
382 process is thought to result from the hydraulic gradient driven by the density difference  
383 between the premelt and the surrounding ice crystals (Rempel, 2005, 2002). Similar facies  
384 have been described close to the ice-bedrock interface of high altitude alpine glaciers (“clear  
385 ice” facies – in Hubbard et al., 2000; Tison and Hubbard, 2000) and at the margin of the  
386 Greenland Ice Sheet (“clotted ice” facies in Sugden et al., 1987; “dispersed with clots” facies in  
387 Souchez et al., (1988, 1993)).

388 The CIS ice type has preserved its water stable isotope signature and is the meteoric ice the  
389 closest to the ice-bedrock interface. It might therefore be considered as a better reference for  
390 the meltwater source to potential refrozen ice types, as compared to the whole set of MI300  
391 samples. However, since folding could have brought meteoric ice from higher up in the ice  
392 sheet close to the ice-bedrock interface, we will keep the meteoric ice of the bottom 300  
393 meters (MI300 in Table 1a;  $S_{MWL} = 8.02$ ) as the potential reference for the input water  
394 signature of the melted ice.

#### 395 4.2.3 Debris-Rich Layers (DRL) and Ice with Dispersed debris (IDD)

396 Both the debris weight content (0.4 to 23 %, Fig. 2b) and the debris size distribution (Fig. 3),  
397 with a characteristic peak in coarser sands, gravels and individual rock pebbles up to 4.5 cm  
398 in diameter, preclude an aeolian origin for the particle load of the DRL and IDD ice types.  
399 Indeed, typical individual particle size ranges e.g. at Camp Century Greenland, from 0.04 to 8  
400  $\mu m$  for the aeolian input (Kumai and Langway Jr, 1988). Only ice-bedrock interactions can

401 therefore be held responsible for the incorporation of such large particle sizes in the NEEM  
402 basal ice.

403 These, however, do not have to imply melting-refreezing processes. Several authors  
404 (Anderton, 1974; Echelmeyer and Zhongxiang, 1987; Fitzsimons et al., 1999; Tison et al.,  
405 1993) have discussed mechanisms for mechanical entrainment of debris in basal ice below  
406 the pmp. Basal ice at the NEEM location is at the pmp and phase changes are therefore likely  
407 to occur. Furthermore, the geometrical arrangement of the debris layers (with the repetition  
408 of small-scale alternation of clear ice and debris layers) is more typical of melting-refreezing  
409 processes (*laminated facies* – see e.g. review from Knight, 1997 and Hubbard et al. (2009)),  
410 “cold” mechanical entrainment generally resulting in a more homogeneously mixed ice/debris  
411 facies (the *amber cryofacies* in Hubbard et al., 2009). Where available, the debris-bearing ice  
412 fabrics (Fig. 4, small crystals) also show a single maximum fabric, typical for ice originating in  
413 the vicinity of the ice-bedrock interface. There, simple shear dominates, rather than the  
414 vertical small girdle resulting from long-term recrystallization under progressive burying in  
415 pure shear regime (Fig. 4, large crystals) close to the pmp. Finally, a maximum difference of  
416 3.5 ‰ is observed between the highest  $\delta^{18}\text{O}$  values in the CIS (-37.9 ‰) and the isotopically  
417 heavier debris-bearing ice sample (-34.4 ‰). This difference is close to the maximum 3 ‰  
418 enrichment in  $\delta^{18}\text{O}$  for oxygen fractionation between ice and water (O’Neil, 1968). It thus  
419 provides further support to a M/R origin for that group. Note that the slightly higher range  
420 may also result from multiple M/R events over successive small bumps, a process known to  
421 produce laminations (Hubbard and Sharp, 1993).

422 Do the co-isotopic signature of the debris-bearing (DRL + IDD) ice types further support a  
423 M/R origin? Figure 5b and Figure 5c show DRL as red triangles and IDD as green squares  
424 respectively. Calculating a regression slope for these two groups together (Debris Bearing ice  
425 in Table 1a, not shown in Figure 5) gives a slope ( $S_{\text{obs-DB}} = 6.47$ , not shown in Figure 5)  
426 identical to the one of the whole basal ice sequence ( $S_{\text{obs-BIWHOLE}} = 6.48$ ), which is significantly  
427 lower than  $S_{\text{MI300}}$  (8.02), and suggesting potential melting-refreezing. The slope is also  
428 significantly too high (P-value = 0) when compared to the one expected for a closed system  
429 M/R ( $S_{\text{CS-DB}} = 5.26$ ) with  $\delta^{18}\text{O}_{\text{res}}$  and  $\delta\text{D}_{\text{res}}$  being the intersection of the regression lines of  
430 debris bearing ice and MI300 groups. Regressions through each individual group (not shown  
431 in Figure 5) give a slightly higher slope for the DRL samples (6.91) and slightly lower slope  
432 (6.27) for the IDD samples, still precluding closed system refreezing.

433 Closer examination of the behaviour of the debris-bearing samples (Fig. 5 b and c) suggests  
434 that an inflexion point exists in the overall trend between heavier and lighter samples at about  
435 -38 ‰, -296 ‰ for  $\delta^{18}\text{O}$  and  $\delta\text{D}$  respectively, in other words, close to the transition from HT  
436 drill samples to rock drill samples (Fig. 2). This is where resistance to drilling penetration  
437 reveals a transition to thicker frozen sediments with larger clasts and interstitial clear ice  
438 layers of the IDD type (Fig. 1c and 3). Restricting the regression calculation to IDD samples  
439 with  $\delta^{18}\text{O} > -38.0$  ‰ (i.e. all IDD samples but one within the ice lenses of the frozen sediments  
440 in the bottom part of the core) gives an observed slope of 5.62 (Table 1a, Figure 5c), which is  
441 significantly different (P-value = 0.01) from  $S_{\text{MI300}}$  (8.02) but not from the theoretical slope (P-  
442 value = 1) calculated using the intersection of the observed regression line with the MWL  
443 (5.28, Table 1b). IDD segments within the frozen sediment at the base of the NEEM core  
444 typically represent closed system refreezing. Note that the isotopic values of the initial water  
445 for these samples (-39.2 ‰; -305 ‰) still lies in the range of the CIS samples (open blue  
446 symbols in Fig. 5a).

447 The DRL samples with  $\delta^{18}\text{O} > -38.0$  ‰ (6.44, Table 1a, Figure 5b) show significant  
448 discrepancy with the MI300 line, but also with the theoretical slope (5.23, Table 1b), ruling

449 out closed system freezing. Since a clear regression line ( $R^2 = 0.97$ ) can be drawn through that  
450 group of samples, an open system freezing process can be considered, as shown below.

451 Using eq. (2) with a) initial water values at the intersection of the regression of DRL samples >  
452  $-38.0\text{‰}$  and MI300 (Table 1b,  $\delta^{18}\text{O} = -40.2\text{‰}$ ,  $\delta\text{D} = -312\text{‰}$ ), b) the observed slope of 6.45,  
453 and c) varying A/F ratio from 1 (input equals amount of freezing) to 10 (freezing is only 10 %  
454 of input), we can reconstruct the range of plausible isotopic values for the input water in the  
455 open system hypothesis (Table 2). The expected isotopic range ( $-42.2\text{‰}$  to  $-40.4\text{‰}$  in  $\delta^{18}\text{O}$ , -  
456  $327\text{‰}$  to  $-313\text{‰}$  in  $\delta\text{D}$ ) is slightly below the lightest CIS ice sample ( $-39.9\text{‰}$  in  $\delta^{18}\text{O}$ ), but  
457 still in the range of the values observed within the last 50 meters of meteoric ice (MI) above  
458 the sampled basal ice sequence (Fig. 5a).

459 As underlined in sect. 3, the geometrical arrangement of the debris layers in the basal ice  
460 sequence (Fig. 4) suggests active folding, in accordance with folding reported higher up in the  
461 core (Dahl-Jensen et al., 2013). It is therefore likely that folding has also affected the few tens  
462 of meters of deep ice above the basal ice layer, providing opportunities for that ice to melt  
463 close to the ice-bedrock interface, somewhere upstream of the drill location, and feeding into  
464 the water reservoir for the “open system” refreezing of the debris rich layers.

465 Both the DRL and the IDD with isotopic values below ( $-38.0\text{‰}$ ;  $-296\text{‰}$ ) do not show a slope  
466 of their regression line (respectively 7.24 in Figure 5b and 7.52 in Figure 5c, Table 1b)  
467 significantly different from that of the MWL (MI300, with P-values of respectively 0.1 and 1).  
468 This suggests that within the debris-rich HT section of the basal ice sequence containing  
469 relatively less debris, mixing processes between the DRL/IDD ice types and the CIS has  
470 destroyed the specific co-isotopic M/R signatures, even at the high (2 cm) sampling resolution  
471 for IDD. Several mechanisms have been invoked for these small-scale mixing processes  
472 between ice and debris close to the ice-bedrock interface. Boulton (1970) proposed that  
473 individual particles or aggregates are incorporated within the flowing ice by undetectable  
474 small-scale melting-refreezing events in the subglacial water film. Small-scale mixing higher  
475 up in the sequence could also result from tectonic thrusting of DRL or IDD layers into the  
476 surrounding CIS layer during a folding event. Such an incorporation process of debris in ice by  
477 tectonic thrusting along shear planes oblique to the layering, in the vicinity of a bedrock  
478 hummock, has been proposed for several basal ice sequences (e.g. Boulton, 1975; Echelmeyer  
479 and Zhongxiang, 1987; Fitzsimons et al., 1999; Tison et al., 1993). More recently, Waller et al.  
480 (2000) and Cook et al. (2011) also underlined the potentially important role of tectonic  
481 mixing in the generation and metamorphism of basal ice sequences.

482 To summarize, our co-isotopic investigations show that: a) melting-refreezing has been  
483 involved in the genesis of the debris-rich layers and the ice with dispersed debris, b) that this  
484 original signature only appears at high-resolution sampling (2 cm) and has only been  
485 preserved in the lower rock-drill section of the basal ice sequence, c) that, in that case, IDD  
486 results from closed system freezing, while an open system freezing is required for DRL  
487 samples and d) that the specific M/R isotopic signature for both DRL and IDD samples is lost  
488 through small-scale mixing ( $< 5$  to 2 cm) in the higher section of the basal ice sequence.

489 The ice crystallography within the DRL shows small crystals and a near vertical c-axes single  
490 maximum (Fig. 4), in accordance with dominant simple-shear in the deeper part of the ice  
491 sheet. The debris content has prevented recrystallization processes in these layers, which act  
492 as discrete weaker zones for accumulated stress release, preventing the inherited  
493 recrystallization fabric of the surrounding CIS from crystal size reduction. A similar pattern  
494 has been described by Tison et al. (1994) in the upper meter of the GRIP core basal ice  
495 sequence.



496 The relatively higher TGC observed in the debris-bearing ice (DRL+IDD) as compared to the  
497 CIS (Fig. 3), may reflect the downward expulsion of the air content from the CIS facies and the  
498 subsequent enrichment of the subglacial water prone to refreeze, sometimes in closed system  
499 configuration (IDD).

#### 500 **4.3 A scenario for the build-up of the NEEM basal ice sequence**

501 The mean  $\delta^{18}\text{O}$  value of the NEEM basal ice sequence (-38.4 ‰) is within the range of the  
502 meteoric ice above, intermediate between Holocene and Younger Dryas values.  
503 Reconstructing the local mean surface temperature using Johnsen et al. (1992) relationship  
504 ( $\delta^{18}\text{O} = 0.67 T - 13.7$  ‰) gives a value of -36.8 °C, compatible with the existence of an  
505 extensive Greenland Ice Sheet. Previously depicted mixing processes between relict low-  
506 altitude ice bodies and a nascent growing ice sheet, such as those invoked for the basal ice at  
507 the GRIP location (Souchez and Jouzel, 2006; Souchez et al., 1995; Tison et al., 1998) are  
508 therefore not applicable for the build-up of the NEEM basal ice sequence. Its origin must  
509 instead be interpreted in terms of incorporation processes of bedrock inherited material  
510 within englacial ice, that occurred under a pre-existing large ice mass. On the basis of the ice  
511 types analysis of the previous section and of the relevant literature, we propose a possible  
512 mechanism for the construction of the NEEM basal ice layers, as depicted in Fig. 7.

513 While snow accumulates and compacts under its own weight to become ice, it simultaneously  
514 undergoes a dry recrystallization process due to the increase of pressure according to depth  
515 (Alley, 1992). At the NEEM location, ice flows NW along the divide and the original  
516 stratigraphy of the deepest layers is shown to be already disturbed by folding at the last  
517 glacial-Eemian boundary (2200 - 2450 m; Dahl-Jensen et al., 2013). Closer to the ice-bedrock  
518 interface, and thanks to the increased recrystallization at temperatures close to the **pmp**,  
519 impurities (including gases) are gathered at crystal boundaries. As described for the deep ice  
520 at EPICA Dome C (de Angelis et al., 2013; Tison et al., 2015) increased concentration of  
521 atmospheric-borne impurities at the grain boundaries leads to the precipitation of salts and to  
522 the aggregation of visible specks. Depending on the amplitude of the bedrock irregularities,  
523 gas expelled within the ice premelt layer will be drained off at the interface with the  
524 intergranular water as a result of density contrast (Rempel, 2001, Tison et al., 2015). At NEEM  
525 this gas loss (clear ice, no specks, Fig. 7, #1) precedes the apparition of visible specks. As the  
526 latter appear, the CIS (Fig. 7, #2) is created, which nonetheless preserves its inherited fabrics  
527 (small girdle around the vertical) and original meteoric signature ( $S_{\text{CIS}} = 7.93$ ), because no  
528 large scale refreezing is involved.

529 Pressure-melting on the stoss side of bedrock hummocks will produce interfacial meltwater  
530 that will flow over and within the basal **till**, eventually entraining fine abrasion products.  
531 Following the pressure gradient, this water will refreeze on the lower pressure lee-side of the  
532 obstacle (Kamb, 1970; Weertman, 1964). This will result in the repetition of millimetric  
533 laminations of debris-rich and clear regelation ice layers such as what has been described  
534 here as our DRL ice type (dark obliquely hatched layers in Fig. 7).

535 Our isotopic analyses show that the refreezing process may occur in an open system regime,  
536 with meltwater contribution from meteoric ice above the CIS horizon, having reached the  
537 bedrock (and partially melted) upstream of the NEEM drilling location. During this open  
538 system refreezing, most of the gases remain dissolved into the water reservoir, although the  
539 TGC of DRL is slightly higher ( $2\text{-}6 \text{ ml}_{\text{gas}} \text{ kg}_{\text{ice}}^{-1}$ , Fig. 2c) than in the CIS layer above. The newly  
540 formed DRL show a c-axes distribution in accordance with the simple shear stress regime  
541 dominant at the base of the ice sheet (single maximum fabric), and their texture made of small

542 crystals reflects the inhibition of their normal grain growth from the presence of debris (Alley  
543 et al., 1986).

544 While the melting-refreezing DRL have to be formed at the ice-sediment interface, several  
545 processes have been proposed to explain their occurrence higher up in the basal ice sequence.  
546 For example, it has been suggested that divergent plastic flow on the stoss side of larger  
547 bedrock obstacles may entrain pre-existing DRL into the superincombent ice layers. By  
548 repetition of the process, numerous DRL can be intercalated within the CIS, as observed in the  
549 top part of our basal ice layer (2533.85 to 2537.30 m). Boulton (1970) stated that, in this  
550 process, the uppermost debris layers are the first to be incorporated at the farthest point up-  
551 flow and the lowest debris layers more locally derived. However, the variability and reverse  
552 directions of the dip of some of the DRL in our sequence suggest that the latter has been  
553 folded. This is consistent with the detailed radio-echosounding observations of Dahl-Jensen et  
554 al. (2013, fig. S2-b and d). Tison et al. (1993) suggest that local shear stress parallel to the  
555 local ice-sediment interface, but oblique to the DRL layering, contributes to its protrusion  
556 within the ice above and to the development of folds across the layering. This can happen at  
557 the interface and help initial incorporation of the DRL (Fig. 7, #3), or further up in the  
558 sequence with previously incorporated DRL (Fig. 7, #3'). This complex deformational regime  
559 will result in small-scale mixing with spatial redistribution of the DRL debris within the  
560 surrounding CIS, resulting in the formation of clear IDD, with a somewhat blurred co-sotopic  
561 signature (Fig. 7, #4).

562 Finally, part of the basal meltwater flowing at the ice-bedrock interface may progressively  
563 infiltrate the pore network of the basal till. If the required temperature and pressure  
564 conditions are met, the refreezing of that water builds up the isolated layers/lenses of IDD  
565 within the frozen sediment, as a kind of segregation ice in permafrost (Fig. 7, #5). This ice  
566 displays an indisputable closed system M/R origin. If it is formed in closer vicinity of the ice-  
567 sediment interface (Fig. 7, #5') it will also dilute its specific isotopic signature within the CIS  
568 meteoric signal (Fig. 4, green squares with  $\delta^{18}\text{O} < -38.0 \text{‰}$ ) as a result of small-scale shearing  
569 and/or folding. A TGC of up to  $60 \text{ ml}_{\text{gas}} \text{ kg}_{\text{ice}}^{-1}$  in the IDD of the lower basal ice section is  
570 coherent with a closed system refreezing process, recovering most of the gas content  
571 originally expelled from the meteoric ice towards the subglacial water system.

## 572 **5 Conclusions**

573 This multiparametric study of the NEEM basal ice sequence has provided, to our best  
574 knowledge, the first opportunity to describe the full transition from unaltered meteoric ice to  
575 frozen basal till, including all intermediary stages. Souchez et al. (2000) argued that  
576 incorporation of relict ice by overriding during initial ice sheet growth is an important process  
577 of basal ice formation in central Greenland. Here, we demonstrate that this situation is not  
578 relevant to NEEM, which needs to be interpreted in terms of formation and transformation  
579 processes occurring under a well developed ice sheet. The full sequence involves the following  
580 succession on the vertical: a) clear ice with normal TGC and no specks, b) clear ice with low  
581 TGC and no specks, c) clear ice with low TGC and specks, d) laminated debris-rich layers and  
582 e) clear ice with dispersed debris, that can either occur as segregation ice within the frozen  
583 sediment of the lower part of the sequence or, higher up in the sequence, as a mix between  
584 clear ice with specks and lower DRL.

585 CIS shows large ice crystals, no signs of melting-refreezing, a pure shear recrystallization  
586 fabric similar to the Eemian ice above and a low debris content with a narrow distribution of  
587 silts and fine sands. It can be compared to the EPICA Dome C basal ice sequence (de Angelis et  
588 al., 2013; Tison et al., 2015) apart from the fact that it already shows a near complete loss of  
589 TGC, suggesting transit closer to bedrock hummocks. Note that EPICA Dome C was stopped

590 some 20 meters above the ice-bedrock interface (Tison et al., 2015). As in EPICA Dome C, the  
591 visible specks are homogeneously dispersed into the ice matrix, with increasing number and  
592 sizes downwards. Therefore they most likely represent autochthonous dissolved impurity  
593 redistribution at crystal boundaries, with intense recrystallization and formation of salt  
594 precipitates.

595 With their tail of coarse sands and gravels and total debris content of up to 23 % (similar to  
596 those of the basal ice of the Byrd Antarctic core, 12-15 %), DRL and IDD cannot result from  
597 aeolian incorporation at the ice sheet surface. This implies thermodynamic (melting-  
598 refreezing, co-isotopic signature) and/or dynamic (folds, layer dips, single maximum ice  
599 fabric) protrusion of basal sediments within the basal ice sequence. This has been described  
600 at length in the literature, such as the basal banded series in West Greenland where  
601 “stratified facies” (dark laminations of sandy debris and clear ice) are interspersed with  
602 “dispersed facies” (clear ice containing fine debris aggregates of silts and clays, also referred  
603 to as “clotted ice”) segments (e.g. Sugden et al., 1987; Souchez et al., 1993).

604 Single maximum ice fabrics in the DRL concord with generalized simple shear conditions close  
605 to the ice bedrock interface. Melting-refreezing at the ice-bedrock interface of NEEM is  
606 coherent with measured temperatures close to the PMP and the upwelling of meltwater in the  
607 drill hole on extraction. Finally, gases rejected from the recrystallized meteoric ice above,  
608 accumulate within the water-soaked sediment below and can be re-incorporated within the  
609 refrozen ice layers, especially if these are formed in a closed system configuration.

610 **Complementary ongoing work within the NEEM basal ice will enable us to further validate  
611 and refine the basal ice build-up processes presented here: for example, gas composition and  
612 isotopic measurements will highlight potential phase changes and biological fractionation  
613 processes, and dating attempts will eventually confirm that the build-up occurred under an  
614 already existing and mature ice sheet, and help refining the succession of events.**

615

## 616 **Acknowledgments**

617 We thank all the participants of the NEEM project. NEEM is directed and organised by the  
618 Center of Ice and Climate at the Niels Bohr Institute and US NSF, Office of Polar Programs. It is  
619 supported by funding agencies and institutions in Belgium (FNRS-CFB and FWO), Canada  
620 (NRCan/GSC), China (CAS), Denmark (FIST), France (IPEV, CNRS/INSU, CEA and ANR),  
621 Germany (AWI), Iceland (RannIs), Japan (NIPR), Korea (KOPRI), The Netherlands  
622 (NWO/ALW), Sweden (VR), Switzerland (SNF), United Kingdom (NERC) and the USA (US NSF,  
623 Office of Polar Programs).

624 T.G. acknowledges support of a FNRS (National Science Foundation, Belgium) - FRIA grant  
625 (5.2.014.15) by the time the present work was conducted. **Finally, the authors are very  
626 grateful to O. Eisen, P. G. Knight and S. Cook for their supportive and constructive comments  
627 on earlier versions of this manuscript.**

628

## 629 **References**

630 Alley, R. B.: Flow law hypotheses for ice-sheet modeling, *J. Glaciol.*, 38(129), 245–256,  
631 1992.

632 Alley, R.B., Lawson, D.E., Evenson, E.B., Strasser, J.C., Larson, G.J., 1998. Glaciohydraulic  
633 supercooling: a freeze-on mechanism to create stratified, debris-rich basal ice: II. Theory.  
634 *Journal of Glaciology* 44, 563–569.

635 Alley, R. B., Perepezko, J. H. and Bentley, C. R.: Grain growth in polar ice: II. Application,  
636 *J. Glaciol.*, 32(112), 425–433, 1986.

637 Andersen, K., Azuma, N. and Barnola, J.-M.: High-resolution record of Northern  
638 Hemisphere climate extending into the last interglacial period, *Nature*, 431(7005), 147–151,  
639 doi:10.1038/nature02805, 2004.

640 Anderton, P. W.: Ice fabrics and petrography, Meserve Glacier, Antarctica, *J. Glaciol.*,  
641 13(68), 285–306, 1974.

642 De Angelis, M., Tison, J. L., Morel-Fourcade, M. C. and Susini, J.: Micro-investigation of  
643 EPICA Dome C bottom ice: Evidence of long term in situ processes involving acid-salt  
644 interactions, mineral dust, and organic matter, *Quat. Sci. Rev.*, 78, 248–265,  
645 doi:10.1016/j.quascirev.2013.08.012, 2013.

646 Bachmann, F., Hielscher, R. and Schaeben, H.: Texture Analysis with MTEX – Free and  
647 Open Source Software Toolbox, *Solid State Phenom.*, 160(2010), 63–68,  
648 doi:10.4028/www.scientific.net/SSP.160.63, 2010.

649 Boulton, G. S.: On the origin and transport of englacial debris in Svalbard glaciers, *J.*  
650 *Glaciol.*, 9(56), 213–229, 1970.

651 Boulton, G. S.: Processes and patterns of subglacial sedimentation: a theoretical approach, in  
652 *Ice Ages: Ancient and Modern*, edited by A. Wright and F. Moseley, pp. 7–42, Seel House  
653 Press Liverpool., 1975.

654 Christoffersen, P., Tulaczyk, S., 2003b. Thermodynamics of basal freeze-on: predicting basal  
655 and subglacial signatures of stopped ice streams and interstream ridges. *Annals of Glaciology*  
656 36, 233–243.

657 Christoffersen, P., Tulaczyk, S., Carsey, F.D., Behar, A.E., 2006. A quantitative framework for  
658 interpretation of basal ice facies formed by ice accretion over subglacial sediment. *Journal of*  
659 *Geophysical Research-Earth Surface* 111. F01017, doi:10.1029/2005JF000363

660 Church, J. a., Clark, P. U., Cazenave, A., Gregory, J. M., Jevrejeva, S., Levermann, A.,  
661 Merrifield, M. a., Milne, G. a., Nerem, R. ., Nunn, P. D., Payne, A. J., Pfeffer, W. T.,  
662 Stammer, D. and Unnikrishnan, A. S.: Sea level change, in *Climate Change 2013: The*  
663 *Physical Science Basis. Contribution of Working Group I to the Fifth Assessment Report of*  
664 *the Intergovernmental Panel on Climate Change*, pp. 1137–1216., 2013.

665 Cook, S.J., Knight, P.G., Waller, R.I., Robinson, Z.P., Adam, W.G., 2007. The geography of basal  
666 ice and its relationship to glaciohydraulic supercooling: Svínafellsjökull, southeast Iceland.  
667 *Quaternary Science Reviews* 26, 2309–2315.

668 Cook, S.J., Robinson, Z.P., Fairchild, I.J., Knight, P.G., Waller, R.I. and Boomer, I., 2009. Role of  
669 glaciohydraulic supercooling in the formation of stratified facies basal ice: Svínafellsjökull and  
670 Skaftafellsjökull, southeast Iceland Article first published online: 4 AUG 2009, p. 24-38, doi:  
671 [10.1111/j.1502-3885.2009.00112](https://doi.org/10.1111/j.1502-3885.2009.00112)

672 Craig, H.: Isotopic Variations in Meteoric Waters., *Science* (80-. ), 133(3465), 1702–1703,  
673 doi:10.1126/science.133.3465.1702, 1961.

674 Cuffey, K. M. and Paterson, W. S. B.: Grain-Scale Structures and Deformation of Ice, in *The*  
675 *physics of glaciers*, Fourth Edition, pp. 29–89, Academic Press., 2010.

676 Dahl-Jensen, D., Albert, M. R., Aldahan, A., Azuma, N., Balslev-Clausen, D., Baumgartner,  
677 M., Berggren, A.-M., Bigler, M., Binder, T., Blunier, T., Bourgeois, J. C., Brook, E. J.,  
678 Buchardt, S. L., Buizert, C., Capron, E., Chappellaz, J., Chung, J., Clausen, H. B., Cvijanovic,  
679 I., Davies, S. M., Ditlevsen, P., Eicher, O., Fischer, H., Fisher, D. a., Fleet, L. G., Gfeller, G.,  
680 Gkinis, V., Gogineni, S., Goto-Azuma, K., Grinsted, A., Gudlaugsdottir, H., Guillevic, M.,  
681 Hansen, S. B., Hansson, M., Hirabayashi, M., Hong, S., Hur, S. D., Huybrechts, P., Hvidberg,  
682 C. S., Iizuka, Y., Jenk, T., Johnsen, S. J., Jones, T. R., Jouzel, J., Karlsson, N. B., Kawamura,  
683 K., Keegan, K., Kettner, E., Kipfstuhl, S., Kjær, H. a., Koutnik, M., Kuramoto, T., Köhler,  
684 P., Laepple, T., Landais, A., Langen, P. L., Larsen, L. B., Leuenberger, D., Leuenberger, M.,  
685 Leuschen, C., Li, J., Lipenkoy, V., Martinerie, P., Maselli, O. J., Masson-Delmotte, V.,  
686 McConnell, J. R., Miller, H., Mini, O., Miyamoto, A., Montagnat-Rentier, M., Mulvaney, R.,  
687 Muscheler, R., Orsi, a. J., Paden, J., Panton, C., Pattyn, F., Petit, J.-R., Pol, K., Popp, T.,  
688 Possnert, G., Prié, F., Prokopiou, M., Quiquet, A., Rasmussen, S. O., Raynaud, D., Ren, J.,  
689 Reutenauer, C., Ritz, C., Röckmann, T., Rosen, J. L., Rubino, M., Rybak, O., Samyn, D.,  
690 Sapart, C. J., Schilt, A., Schmidt, a. M. Z., Schwander, J., Schüpbach, S., Seierstad, I., et al.:  
691 Eemian interglacial reconstructed from a Greenland folded ice core, *Nature*, 493(7433), 489–  
692 494, doi:10.1038/nature11789, 2013.

693 Echelmeyer, K. and Zhongxiang, W.: Direct observation of basal sliding and deformation of  
694 basal drift at sub-freezing temperatures, *J. Glaciol.*, 33(113), 83–09, 1987.

695 Fischer, H., Severinghaus, J., Brook, E., Wolff, E., Albert, M., Alemany, O., Arthern, R.,  
696 Bentley, C., Blankenship, D. and Chappellaz, J.: Where to find 1.5 million yr old ice for the  
697 IPICS“ Oldest Ice” ice core, *Clim. Past Discuss.*, 9(3), 2771–2815, 2013.

698 Fitzsimons, S. J., McManus, K. J. and Lorrain, R. D.: Structure and strength of basal ice and  
699 substrate of a dry-based glacier: evidence for substrate deformation at sub-freezing  
700 temperatures, *Ann. Glaciol.*, 28(1), 236–240, 1999.

701 Friedman, I., Redfield, A. C., Schoen, B. and Harris, J.: The variation of the deuterium  
702 content of natural waters in the hydrologic cycle, *Rev. Geophys.*, 2(1), 177–224, 1964.

703 Gow, A. and Meese, D.: Nature of basal debris in the GISP2 and Byrd ice cores and its  
704 relevance to bed processes, *Ann. Glaciol.*, 1996.

705 Hooke, R. L. and Hudleston, P. J.: Ice fabrics in a vertical flow plane, Barnes Ice Cap,  
706 Canada, *J. Glaciol.*, 25, 195–214, 1980.

707 Hubbard, B., Cook, S. and Coulson, H.: Basal ice facies: a review and unifying approach,  
708 *Quat. Sci. Rev.*, 28(19-20), 1956–1969, doi:10.1016/j.quascirev.2009.03.005, 2009.

709 Hubbard, B. and Sharp, M.: Basal ice formation and deformation: a review, *Prog. Phys.*  
710 *Geogr.*, 13(4), 529–558, doi:10.1177/030913338901300403, 1989.

711 Hubbard, B. and Sharp, M.: Weertman regelation, multiple refreezing events and the isotopic  
712 evolution of the basal ice layer, *J. Glaciol.*, 1993.

713 Hubbard, B. and Sharp, M.: Basal ice facies and their formation in the Western Alps, *Arct.*  
714 *Alp. Res.*, 27(4), 301–310, 1995.

715 Hubbard, B., Tison, J. L., Janssens, L. and Spiro, B.: Ice-core evidence of the thickness and  
716 character of clear-facies basal ice: Glacier de Tsanfleuron, Switzerland, *J. Glaciol.*, 46(152),  
717 140–150, doi:10.3189/172756500781833250, 2000.

718 Iverson R., N. and Souchez, R.: Isotopic signature of debris-rich ice formed by regelation  
719 into a subglacial sediment bed, *Geophys. Res. Lett.*, 23(10), 1151–1154,  
720 doi:10.1029/96GL01073, 1996.

721 Johnsen, S. J., Clausen, H. B., Dansgaard, W., Fuhrer, K., Gundestrup, N., Hammer, C. U.,  
722 Iversen, P., Jouzel, J., Stauffer, B. and Steffensen, J. P.: Irregular glacial interstadials  
723 recorded in a new Greenland ice core, *Nature*, 359(6393), 311–313, 1992.

724 Johnsen, S. J., Hansen, S. B., Sheldon, S. G., Dahl-Jensen, D., Steffensen, J. P., Augustin, L.  
725 J., Journé, P., Alemany, O., Rufli, H., Schwander, J., Azuma, N., Motoyama, H., Popp, T.,  
726 Talalay, P. G., Thorsteinsson, T., Wilhelms, F. and Zagorodnov, V.: The Hans Tausen drill:  
727 Design, performance, further developments and some lessons learned, in *Annals of*  
728 *Glaciology*, vol. 47, pp. 89–98., 2007.

729 Jouzel, J. and Souchez, R.: Melting-refreezing at the glacier sole and the isotopic composition  
730 of the ice, *J. Glaciol.*, 28(98), 35–42, 1982.

731 Kamb, B.: Sliding motion of glaciers: theory and observation, *Rev. Geophys.*, 8(4), 673–728,  
732 1970.

733 Knight, P.: Stacking of basal debris layers without bulk freezing-on: isotopic evidence from  
734 West Greenland, *J. Glaciol.*, 35(120), 214 – 216, 1989.

735 Knight, P. G.: The basal ice layer of glaciers and ice sheets, *Quat. Sci. Rev.*, 16(9), 975–993,  
736 doi:10.1016/S0277-3791(97)00033-4, 1997.

737 Kumai, M. and Langway Jr, C. C.: Electron microscope analysis of aerosols in snow and  
738 deep ice cores from Greenland, *Isot. Impurities Snow Ice*, IAHS Publ, 10, 208–, 1988.

739 Landais, a., Dreyfus, G., Capron, E., Pol, K., Loutre, M. F., Raynaud, D., Lipenkov, V. Y.,  
740 Arnaud, L., Masson-Delmotte, V., Paillard, D., Jouzel, J. and Leuenberger, M.: Towards  
741 orbital dating of the EPICA Dome C ice core using  $\delta\text{O } 2/\text{N } 2$ , *Clim. Past*, 8(1), 191–203,  
742 doi:10.5194/cp-8-191-2012, 2012.

743 Langway, C. C.: Ice fabrics and the universal stage, *SIPRE Tech. Rep.*, 62, 1958.

744 Larson, G. J., Lawson, D. E., Evenson, E. B., Knudsen, Ó., Alley, R. B. and Phanikumar, M.  
745 S.: Origin of stratified basal ice in outlet glaciers of Vatnajökull and Öræfajökull, Iceland,  
746 *Boreas*, 39(3), 457–470, doi:10.1111/j.1502-3885.2009.00134.x, 2010.

747 Lehmann, M. and Siegenthaler, U.: Equilibrium oxygen and hydrogen-isotope fractionation  
748 between ice and water, *J. Glaciol.*, 37(125), 23–26, 1991.

749 Lawson, D.E., Strasser, J.C., Evenson, E.B., Alley, R.B., Larson, G.J., Arcone, S.A., 1998.  
750 Glaciohydraulic supercooling: a freeze-on mechanism to create stratified, debris-rich basal ice:  
751 I. Field evidence. *Journal of Glaciology* 44, 547–562.

752 Martinerie, P., Lipenkov, V. Y., Raynaud, D., Chappellaz, J., Barkov, N. I. and Lorius, C.:  
753 Air content paleo record in the Vostok ice core (Antarctica): A mixed record of climatic and  
754 glaciological parameters, *J. Geophys. Res.*, 99(D5), 10565–10576, doi:10.1029/93JD03223,  
755 1994.

756 Montagnat, M., Azuma, N., Dahl-Jensen, D., Eichler, J., Fujita, S., Gillet-Chaulet, F.,  
757 Kipfstuhl, S., Samyn, D., Svensson, a. and Weikusat, I.: Fabric measurement along the  
758 NEEM ice core, Greenland, and comparison with GRIP and NGRIP ice cores, *Cryosph.*  
759 *Discuss.*, 8(1), 307–335, doi:10.5194/tcd-8-307-2014, 2014.

760 O'Neil, J. R.: Hydrogen isotope fractionation between ice and water, *J. Phys. Chem.*, 72(10),  
761 3683–3684, 1968.

762 Peternell, M., Dierckx, M., Wilson, C. J. L. and Piazzolo, S.: Quantification of the  
763 microstructural evolution of polycrystalline fabrics using FAME: Application to in situ  
764 deformation of ice, *J. Struct. Geol.*, 61, 109–122, doi:10.1016/j.jsg.2013.05.005, 2014.

765 Raynaud, D., Delmas, D., Ascencio, J. M. and Legrand, M.: Gas extraction from polar ice  
766 cores: a critical issue for studying the evolution of atmospheric CO<sub>2</sub> and ice-sheet surface  
767 elevation, *Ann. Glaciol.*, 3, 265–268, 1983.

768 Rempel, A.: Englacial phase changes and intergranular flow above subglacial lakes, *Ann.*  
769 *Glaciol.*, 40(1), 191–194, doi:10.3189/172756405781813564, 2005.

770 Rempel, A. W.: Anomalous diffusion of multiple impurity species: Predicted implications  
771 for the ice core climate records, *J. Geophys. Res.*, 107(B12), 2330,  
772 doi:10.1029/2002JB001857, 2002.

773 Souchez, R.: On the isotopic composition in  $\delta D$  and  $\delta^{18}O$  of water and ice during freezing, *J.*  
774 *Glaciol.*, 30(106), 369–372, 1984.

775 Souchez, R. A. and De Groote, J. M.:  $\delta D$ - $\delta^{18}O$  relationships in ice formed by subglacial  
776 freezing: paleoclimatic implications, *J. Glaciol.*, 31(109), 229–232, 1985.

777 Souchez, R. A. and Lorrain, R. D.: *Ice Composition and Glacier Dynamics*, Springer Science  
778 & Business Media., 1991.

779 Souchez, R., Bouzette, A., Clausen, H. B., Johnsen, S. J., Jouzel, J., Clausen B., H., Johnsen  
780 J., S. and Jouzel, J.: A stacked mixing sequence at the base of the Dye 3 core, Greenland,  
781 *Geophys. Res. Lett.*, 25(11), 1943–1946, doi:10.1029/98GL01411, 1998.

782 Souchez, R. and Jouzel, J.: Gas isotopes in ice reveal a vegetated central Greenland during  
783 ice sheet invasion, *Geophys. Res. Lett.*, 33(24), 2–5, doi:10.1029/2006GL028424, 2006.

784 Souchez, R., Lemmens, M. and Chappellaz, J.: Flow-induced mixing in the GRIP basal ice  
785 deduced from the CO<sub>2</sub> and CH<sub>4</sub> records, *Geophys. Res. Lett.*, 22(1), 41–44,  
786 doi:10.1029/94GL02863, 1995.

787 Souchez, R., Lemmens, M., Lorrain, R. and Tison, J.-L.: Pressure-melting within a glacier  
788 indicated by the chemistry of regelation ice, *Nature*, 273(5662), 454–456,  
789 doi:10.1038/273454a0, 1978.



790 Souchez, R., Lemmens, M., Tison, J.-L., Lorrain, R. and Janssens, L.: Reconstruction of basal  
791 boundary conditions at the Greenland Ice Sheet margin from gas composition in the ice, *Earth*  
792 *Planet. Sci. Lett.*, 118(1-4), 327–333, doi:10.1016/0012-821X(93)90176-A, 1993.

793 Souchez, R., Lorrain, R., Tison, J. L., Jouzel, J., Bruxelles, U. L. De, Iouzel, J. and Jouzel,  
794 J.: Co-isotopic signature of two mechanisms of basal-ice formation in Arctic outlet glaciers,  
795 *Ann. Glaciol.*, 10, 163–166, 1988.

796 Souchez, R., Tison, J., Lorrain, R., Lemmens, M., Janssens, L., Stievenard, M., Jouzel, J.,  
797 Sveinbjörnsdóttir, A. and Johnsen, S. J.: Stable isotopes in the basal silty ice preserved in the  
798 Greenland Ice Sheet at Summit; environmental implications, *Geophys. Res. Lett.*, 21(8),  
799 693–696, 1994.

800 Souchez, R., Vandenschrick, G., Lorrain, R. and Tison, J.-L.: Basal ice formation and  
801 deformation in central Greenland: a review of existing and new ice core data, *Geol. Soc.*  
802 *London, Spec. Publ.*, 176(1), 13–22, doi:10.1144/GSL.SP.2000.176.01.02, 2000.

803 Sugden, D. E., Knight, P. G., Livesey, N., Lorrain, R. D., Souchez, R. A., Tison, J.-L. and  
804 Jouzel, J.: Evidence for two zones of debris entrainment beneath the Greenland ice sheet,  
805 *Nature*, 328(6127), 238–241, doi:10.1038/328238a0, 1987.

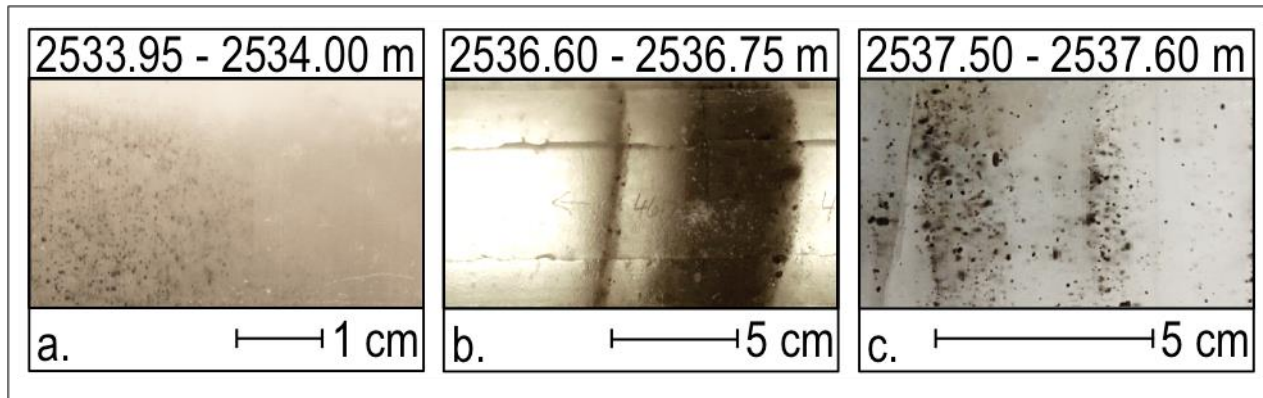
806 Tison, J., Thorsteinsson, T., Lorrain, R. D. and Kipfstuhl, J.: Origin and development of  
807 textures and fabrics in basal ice at Summit, Central Greenland, *Earth Planet. Sci. Lett.*, 125(1-  
808 4), 421–437, doi:10.1016/0012-821X(94)90230-5, 1994.

809 Tison, J.-L.: Diamond wire-saw cutting techniques for investigating textures and fabrics of  
810 debris-laden ice and brittle ice, *J. Glaciol.*, 40(135), 410–414, 1994.

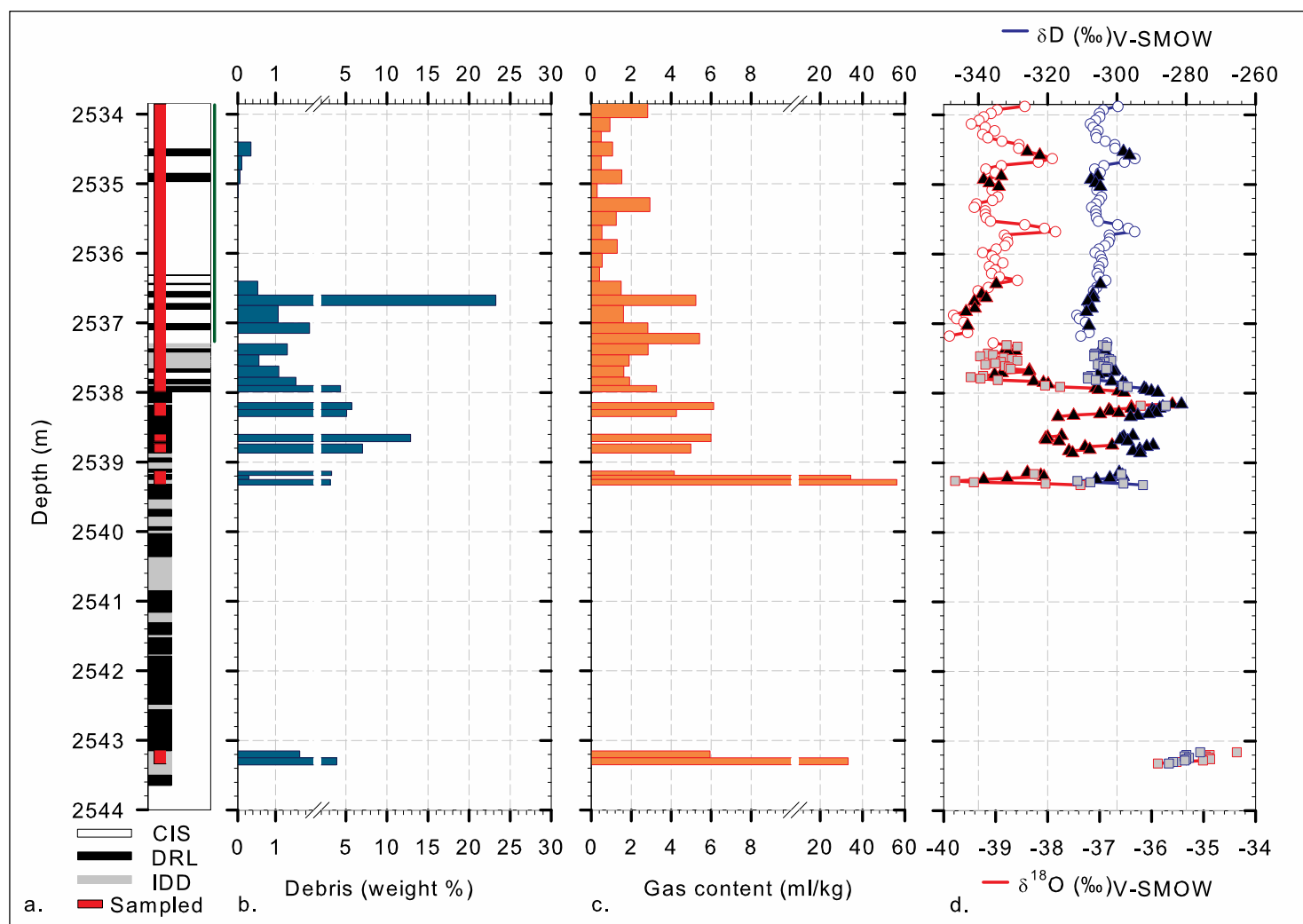
811 Tison, J.-L., de Angelis, M., Littot, G., Wolff, E., Fischer, H., Hansson, M., Bigler, M.,  
812 Udisti, R., Wegner, A., Jouzel, J., Stenni, B., Johnsen, S., Masson-Delmotte, V., Landais, A.,  
813 Lipenkoy, V., Loulergue, L., Barnola, J.-M., Petit, J.-R., Delmonte, B., Dreyfus, G., Dahl-  
814 Jensen, D., Durand, G., Bereiter, B., Schilt, A., Spahni, R., Pol, K., Lorrain, R., Souchez, R.  
815 and Samyn, D.: Can we retrieve a clear paleoclimatic signal from the deeper part of the  
816 EPICA Dome C ice core?, *Cryosph. Discuss.*, 9(1), 567–608, doi:10.5194/tcd-9-567-2015,  
817 2015.

818 Tison, J.-L. and Hubbard, B.: Ice crystallographic evolution at a temperate glacier: Glacier  
819 de Tsanfleuron, Switzerland, *Geol. Soc. London, Spec. Publ.*, 176(1), 23–38, 2000.

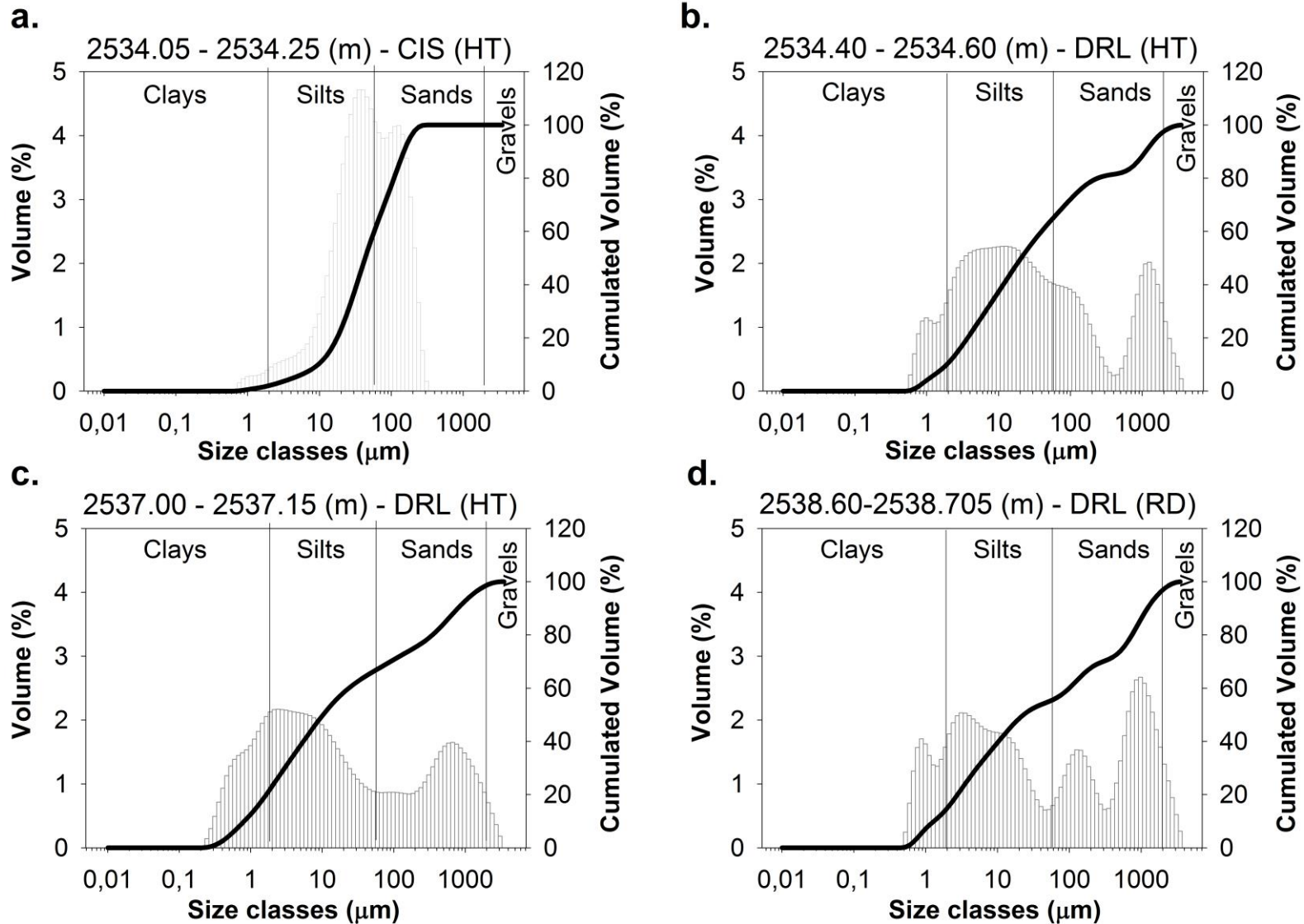
- 820 Tison, J.-L., Petit, J.-R., Barnola, J. M. and Mahaney, W.: Debris entrainment at the ice-  
821 bedrock interface in sub-freezing temperature conditions (Adélie Land, Antarctica), *J.*  
822 *Glaciol.*, 39(132), 303–315, 1993.
- 823 Tison, J.-L., Souchez, R., Wolff, E. W., Moore, J. C., Legrand, M. R. and de Angelis, M.: Is  
824 a periglacial biota responsible for enhanced dielectric response in basal ice from the  
825 Greenland Ice Core Project ice core?, *J. Geophys. Res.*, 103(D15), 18,885–18,894,  
826 doi:10.1029/98JD01107, 1998.
- 827 Weertman, J.: Mechanism for the formation of inner moraines found near the edge of cold  
828 ice caps and ice sheets, *J. Glaciol.*, 3(30), 965–978, 1961.
- 829 Weertman, J.: Glacier sliding, *J. Glaciol.*, 5, 287–303, 1964.
- 830 Wilson, C. J. L., Russell-Head, D. S. and Sim, H. M.: The application of an automated fabric  
831 analyzer system to the textural evolution of folded ice layers in shear zones, *Ann. Glaciol.*,  
832 37(1), 7–17, doi:10.3189/172756403781815401, 2003.



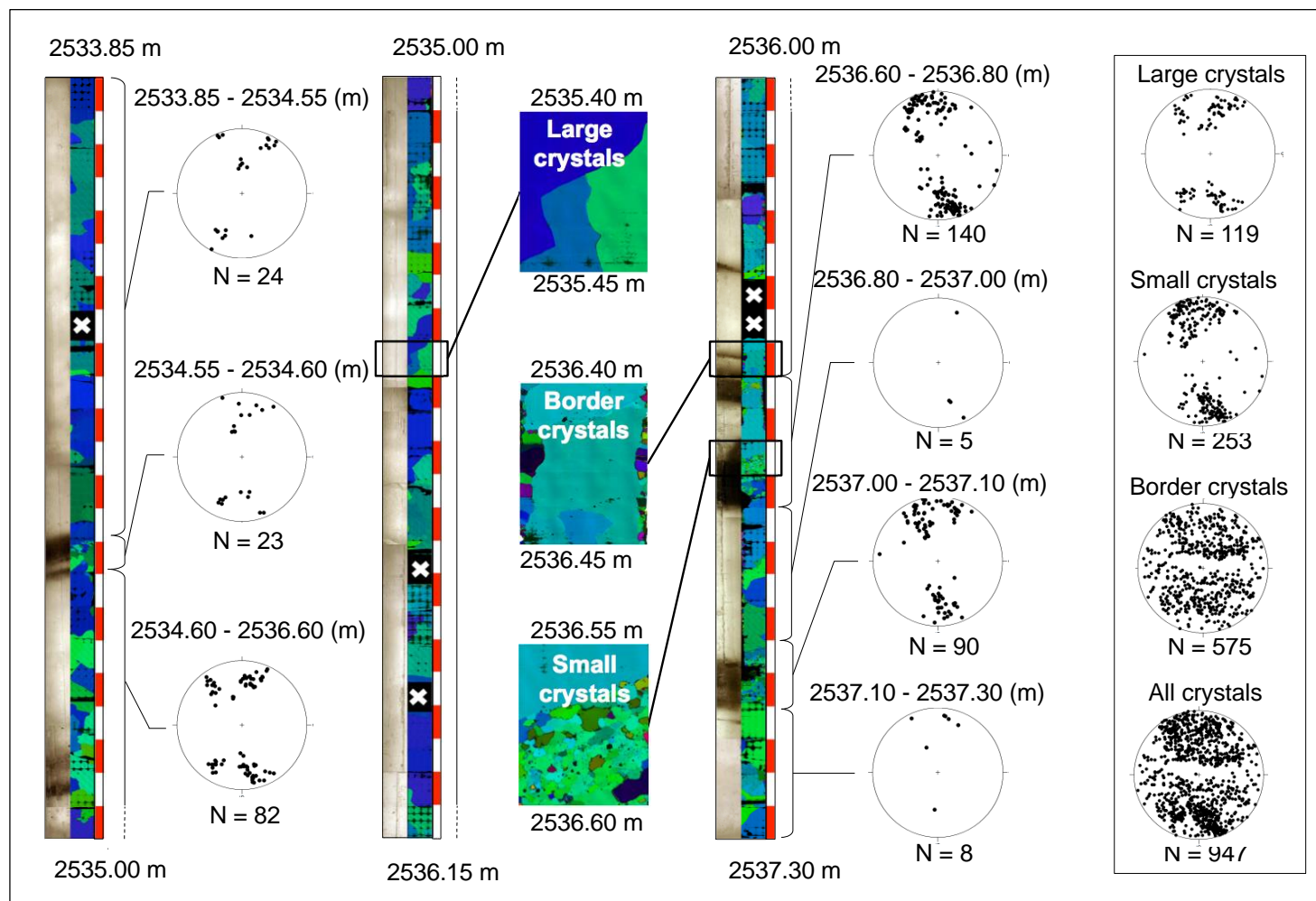
833 **Fig. 1.** Representative photographs of the **the three visually contrasting ice types** encountered in the  
834 NEEM BIL sampled with the HT drill. **a.** clear ice with specks (CIS), **b.** debris rich layers (DRL)  
835 embedded in clear ice, **c.** ice containing dispersed debris (IDD). Note the difference in scales for the  
836 three pictures.



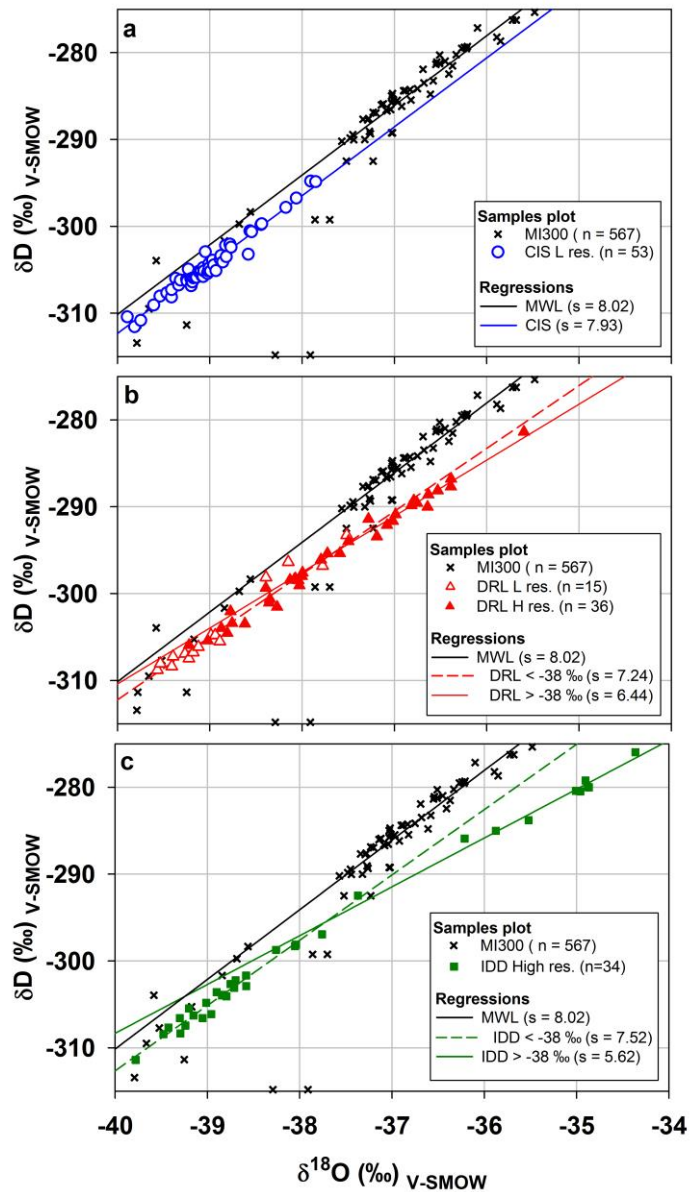
837 **Fig. 2.** Vertical profiles: **a.** symbolic representation of the ice types encountered along the core (CIS, DRL, IDD). The  
 838 green bar corresponds to the part of the core detailed in Fig. 4, **b.** debris content in weight percentage, **c.** Total gas  
 839 content, **d.**  $\delta^{18}O$  (bottom axis, red symbols) and  $\delta D$  (top axis, blue symbols), white circles: CIS, black triangles: DRL,  
 840 grey squares: IDD.



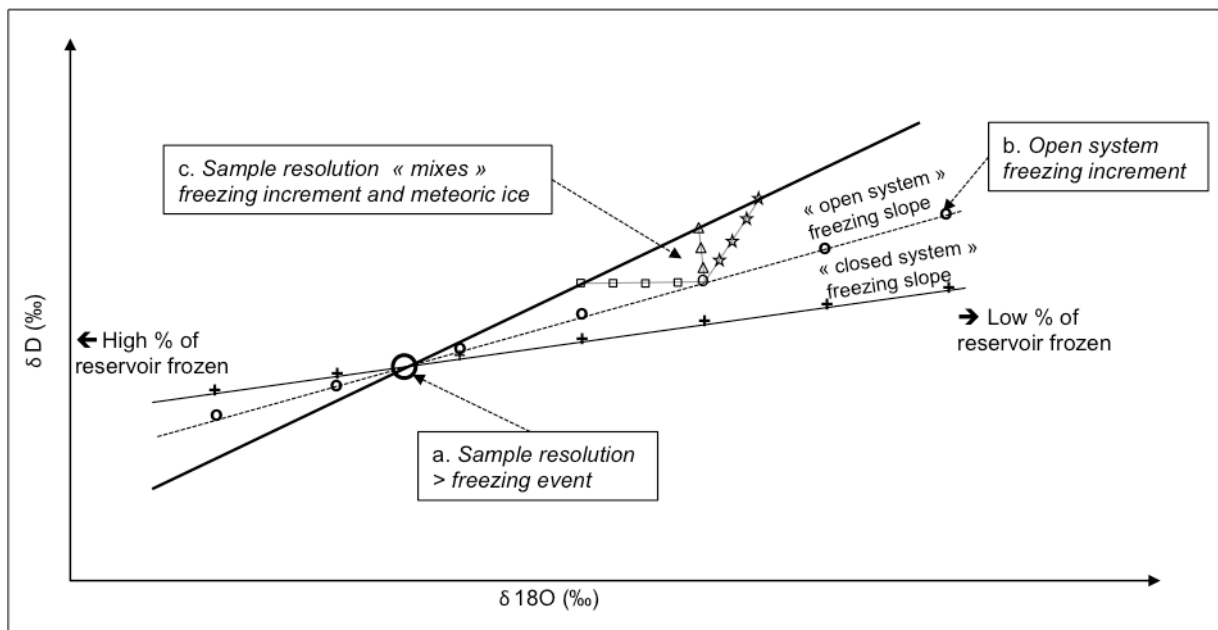
841 **Fig. 3.** Granulometric plots for characteristic samples at increasing depths. Grey vertical bars: volume (%); Black line:  
 842 Cumulated volumes (%).



843 **Fig. 4.** Vertical profile presenting the 2011 season - HT drill cores. From left to right, for each section of the core:  
 844 photographs of the core in transmitted light, vertical thin sections images from the automated ice fabric analyser,  
 845 fabric plots in the vertical plane with associated depth range for the crystals used. The red and white scale units are 5  
 846 cm each. The frame presents the fabrics for crystals grouped by types.

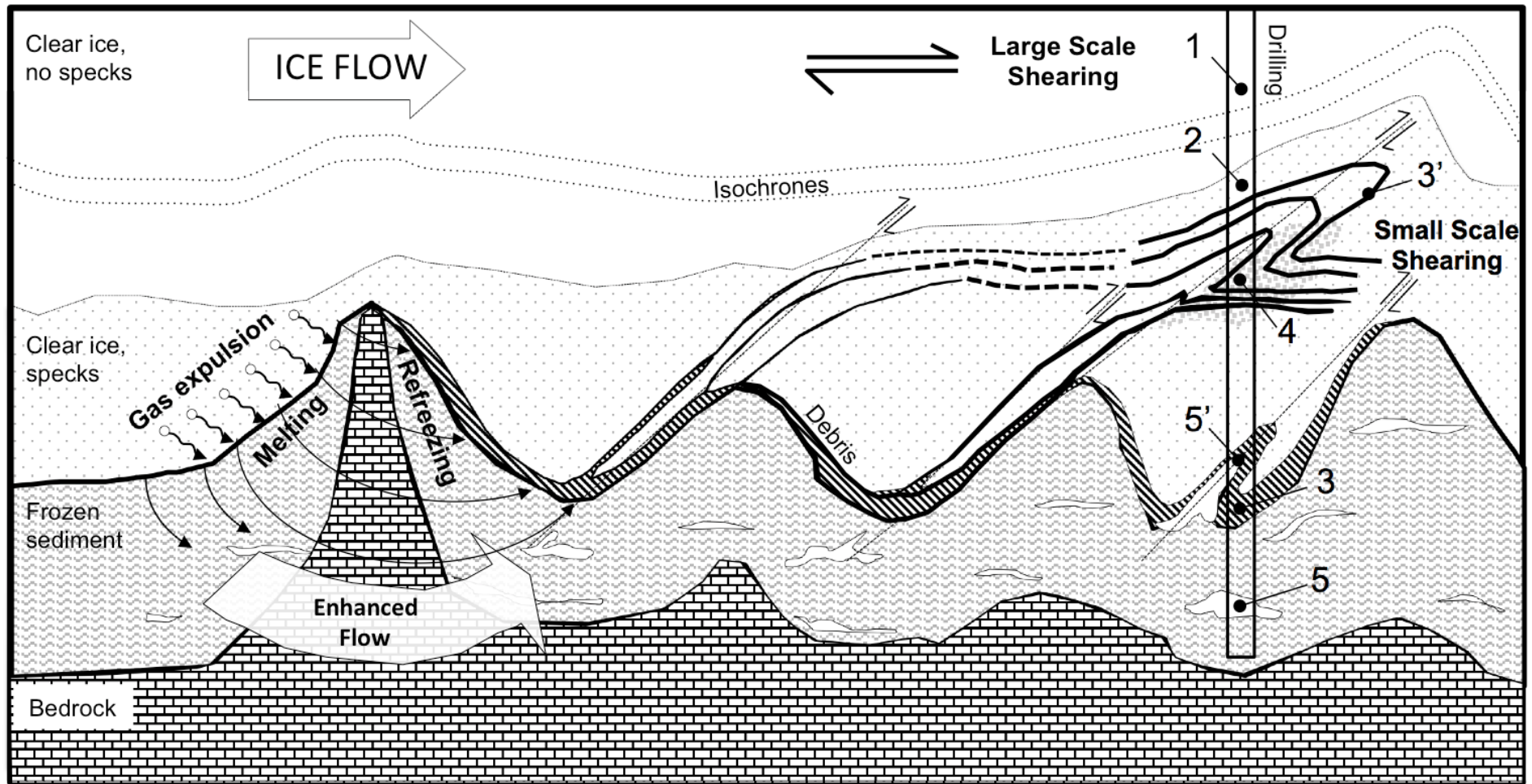


847 **Fig. 5.** Co-isotopic diagram presenting both the last 300 m of meteoric ice (MI300, black crosses) and the basal ice  
 848 samples at the NEEM location. The plots are centered on the BIL range. Open symbols correspond to low vertical  
 849 resolution samples (5 cm) and closed symbols to high vertical resolution samples (2 cm). Lines: regressions for  
 850 investigated groups of samples, n: number of samples of the considered group, s: value of the slope of the regressions.  
 851 5a: CIS (blue circles); 5b: DRL (red triangles); 5c: IDD (green squares). See text for details.



852 **Fig. 6.** Scheme describing the potential isotopic signatures for various combinations of open and  
 853 closed system freezing, mixing and sampling resolution. The black thick line represents the  
 854 Meteoric Water Line.





855 **Fig. 7.** Scheme for the build up of the basal ice sequence at NEEM, based on the interpretation of the observed properties (not to scale). Note that all  
 856 processes may combine at each bedrock bump. See text for for more details and numbers caption.

857

**a. Observed regression line**

Group of samples	Acronym	Slope (Sobs)	Intercept	R <sup>2</sup>	N (number of samples)
Meteoritic Ice from 300m above the basal ice layer	MI300	8.02	10.73	0.99	567
Whole basal ice sequence	BI <sub>whole</sub>	6.48	-51.99	0.98	138
Clear ice with Specks	CIS	7.93	4.95	0.96	53
Debris bearing ice (DRL + IDD)	DB	6.47	-52.57	0.99	85
Debris-Rich Layers	DRL	6.91	-35.60	0.98	51
Ice with Dispersed Debris	IDD	6.27	-60.31	0.99	34
Debris-Rich Layers $\delta^{18}\text{O} > -38\text{‰}$	DRL>38	6.45	-52.61	0.97	20
Debris-Rich Layers $\delta^{18}\text{O} < -38\text{‰}$	DRL<38	7.24	-22.77	0.94	31
Ice with Dispersed Debris $\delta^{18}\text{O} > -38\text{‰}$	IDD>38	5.62	-83.40	0.99	11
Ice with Dispersed Debris $\delta^{18}\text{O} < -38\text{‰}$	IDD<38	7.52	-11.79	0.96	23

**b. Theoretical Closed-system freezing line**

Initial water used for slope calculation ( $\cap$ =intersection)	$\delta^{18}\text{O}$ intercept	$\delta\text{D}$ intercept	Theoretical slope (S <sub>cs</sub> )	Theoretical intercept
BI <sub>whole</sub> $\cap$ MI300	-40.63	-315.24	5.20	1.49
CIS $\cap$ MI300	-64.43	-506.17	3.85	2.04
DRL $\cap$ MI300	-41.48	-322.04	5.15	1.51
IDD $\cap$ MI300	-40.64	-315.27	5.20	1.49
DRL > 38 $\cap$ MI300	-40.17	-311.53	5.23	1.48
DRL < 38 $\cap$ MI300	-42.66	-331.47	5.09	1.53

IDD > 38 ∩ MI300	-39.24	-304.09	5.28	1.47
IDD < 38 ∩ MI300	-45.02	-350.45	4.96	1.57

859 **Table 1. a.** Parameters of regressions, **b.** Theoretical slopes computed using the closed-system model eq. (1).

860

861

A/F	$\delta^{18}\text{O}$	$\delta\text{D}$
1	-42.2	-327
2	-41.2	-319
3	-40.9	-316
4	-40.7	-315
5	-40.6	-315
6	-40.5	-314
7	-40.5	-314
8	-40.4	-314
9	-40.4	-313
10	-40.4	-313

862

863 **Table 2.** Expected range of input water  $\delta$ -values (‰) in an open system freezing configuration computed with the  
864 observed slope of 6.45 and a range of A/F values from 1 to 10.